

แบบจำลองสมการเชิงอนุพันธ์สี่ตัวแคสติกบนทรงกลมสำหรับการอพยพของสัตว์



วิทยานิพนธ์นี้เป็นส่วนหนึ่งของการศึกษาตามหลักสูตรปริญญาวิทยาศาสตรมหาบัณฑิต

สาขาวิชาคณิตศาสตร์ประยุกต์และวิทยาการคณนา

ภาควิชาคณิตศาสตร์และวิทยาการคอมพิวเตอร์

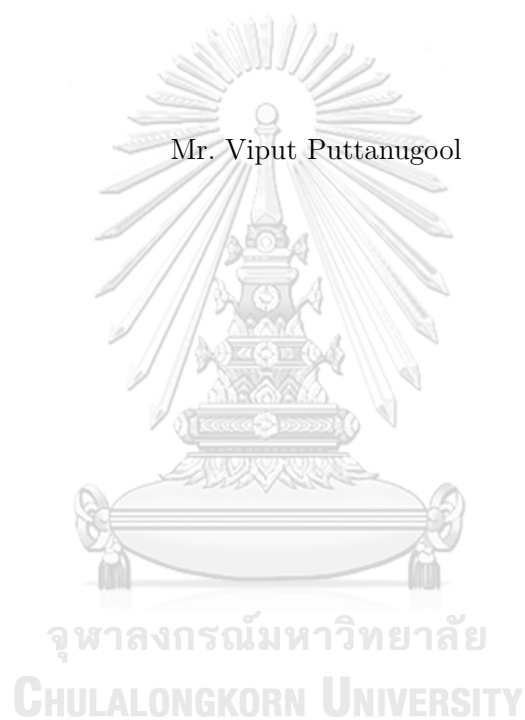
คณะวิทยาศาสตร์ จุฬาลงกรณ์มหาวิทยาลัย

ปีการศึกษา 2563

ลิขสิทธิ์ของจุฬาลงกรณ์มหาวิทยาลัย

STOCHASTIC DIFFERENTIAL EQUATION MODELS ON SPHERE FOR  
ANIMAL MIGRATION

Mr. Viput Puttanugool



A Thesis Submitted in Partial Fulfillment of the Requirements  
for the Degree of Master of Science Program in Applied Mathematics and

Computational Science

Department of Mathematics and Computer Science

Faculty of Science

Chulalongkorn University

Academic Year 2020

Copyright of Chulalongkorn University



วิพุธ พุทธนุกูล : แบบจำลองสมการเชิงอนุพันธ์สโตแคสติกบนทรงกลมสำหรับการอพยพของสัตว์. (STOCHASTIC DIFFERENTIAL EQUATION MODELS ON SPHERE FOR ANIMAL MIGRATION) อ.ที่ปรึกษาวิทยานิพนธ์หลัก : รศ.ดร.คำรณ เมฆฉาย, อ.ที่ปรึกษาวิทยานิพนธ์ร่วม : ดร.เรวัต ถนัดกิจหิรัญ 62 หน้า.

การอพยพของสัตว์คือการเคลื่อนที่ตามฤดูกาลของกลุ่มสัตว์จากสถานที่หนึ่งไปยังสถานที่อื่น วงจรการอพยพของสัตว์มักเกิดขึ้นเป็นประจำทุกปีและมักสอดคล้องกับรูปแบบวัฏจักรของฤดูกาล องค์ความรู้ด้านการอพยพของสัตว์ถูกพัฒนามาอย่างต่อเนื่อง แต่ปัจจุบันยังไม่มีเหตุผลที่ชัดเจนที่จะอธิบายพฤติกรรมการอพยพของสัตว์ และแบบจำลองการอพยพของสัตว์ได้ถูกสร้างขึ้นเพื่อทำนายเส้นทางการอพยพของสัตว์ การอพยพทางไกลสามารถสร้างแบบจำลองบนพื้นผิวระนาบ แต่สัตว์บางชนิดมีการอพยพทางไกลเช่นนก Arctic terns อพยพจากขั้วโลกเหนือไปยังขั้วโลกใต้ ดังนั้นการอพยพของพวกมันควรถูกสร้างแบบจำลองบนพื้นผิวทรงกลม นอกจากนี้พจน์ของการเคลื่อนที่แบบบราวน์ได้ถูกรวมอยู่ในแบบจำลองเพื่อแสดงถึงความคลาดเคลื่อนและพฤติกรรมการเคลื่อนไหวแบบสุ่มของสัตว์ งานวิจัยนี้มีวัตถุประสงค์เพื่อสร้างแบบจำลองการอพยพของสัตว์ และจำลองเส้นทางการอพยพของสัตว์โดยใช้ระบบสมการเชิงอนุพันธ์สโตแคสติก (SDEs) บนทรงกลม และฟังก์ชันพฤติกรรมที่อธิบายพฤติกรรมของสัตว์ในระหว่างการอพยพ แบบจำลองเส้นทางการอพยพของสัตว์ถูกสร้างขึ้นโดย SDEs ที่ผลลัพธ์ลู่เข้าไปสู่จุดบนพื้นผิวระนาบซึ่งถูกแปลงเป็น SDEs ที่ผลลัพธ์ลู่เข้าไปสู่จุดบนพื้นผิวทรงกลม โดยใช้ฟังก์ชันเส้นโค้งแผนที่ที่เหมาะสม การจำลองเส้นทางการอพยพของสัตว์จะถูกสร้างขึ้นโดยใช้ระเบียบวิธีของออยเลอร์-มารูยามะเพื่อแสดงเส้นทางการอพยพของสัตว์

ภาควิชา	คณิตศาสตร์และ	ลายมือชื่อนิสิต
	วิทยาการคอมพิวเตอร์	ลายมือชื่อ อ.ที่ปรึกษาหลัก
สาขาวิชา	คณิตศาสตร์ประยุกต์	ลายมือชื่อ อ.ที่ปรึกษาร่วม
	และวิทยาการคณนา	
ปีการศึกษา	2563	

## ID : MAJOR APPLIED MATHEMATICS AND COMPUTATIONAL SCIENCE

KEYWORDS : ANIMAL MIGRATION / STOCHASTIC DIFFERENTIAL EQUATION

VIPUT PUTTANUGOOL : STOCHASTIC DIFFERENTIAL EQUATION MODELS  
ON SPHERE FOR ANIMAL MIGRATION. ADVISOR : ASSOC. PROF. KHAMRON  
MEKCHAY, Ph.D., THESIS COADVISOR : RAYWAT TANADKITHIRUN, Ph.D., 62  
pp.

Animal migration is a seasonal movement of a bundle of animals from place to place. A migration cycle is often annually and closely linked with the cyclic pattern of seasons. A short-distance migration can be modeled on a planar surface, but most animals have long-distance migrations, e.g., Arctic terns migrate from the North Pole to the South Pole; thus, their migration should be modeled on a spherical surface. In addition, the Brownian motion term is included in a model to represent noises and randomness of movements. This work aims to simulate their migration routes using stochastic differential equations (SDEs) on sphere together with additional behavior functions describing behaviors of animals during their migration. The models are constructed based on SDEs on planar surface whose solution moves toward a particular point which is then transformed to SDEs on sphere using appropriate map projection functions. Finally, the simulations of routes are constructed using the Euler-Maruyama scheme to show animal migration routes.

Department	: .. Mathematics and .....	Student's Signature .....
	.. Computer Science .....	Advisor's Signature .....
Field of Study	: .. Applied Mathematics and .....	Co-advisor's Signature .....
	.. Computational Science .....	
Academic Year	: .. 2020 .....	

## ACKNOWLEDGEMENTS

First and foremost, I would like to express my sincere gratitude to my advisor, Associate Professor Dr. Khamron Mekchay, and my co-advisor Dr. Raywat Tanadkithirun for all support in the master's degree. I further would like to thank all of my committees: Associate Professor Dr. Petarpa Boonserm, Assistant Professor Dr. Boonyarit Intiyot, and Dr. Sirod Sirisup, for their insightful comments and suggestions which motivated me to extend my research from various perspectives. Next, I would like to thank the Development and Promotion of Science and Technology Talents Project (DPST) for financial support and Department of Mathematics and Computer Science, Chulalongkorn University for providing an opportunity to operate this work. Moreover, I wish to show my gratitude to Seabird Tracking Database, BirdLife International, and Carsten Egevang for providing data. I wish to express my deepest gratitude to Thada Udomprapasup for a suggestion on the SDE model of movements of points on a plane and Dr. Ampol Duangpan for a big support. Last but not least, I have to thank my parents, my friends, and everyone surrounding me for all their support throughout the period of this research.

# CONTENTS

	Page
<b>ABSTRACT IN THAI</b> . . . . .	iv
<b>ABSTRACT IN ENGLISH</b> . . . . .	v
<b>ACKNOWLEDGEMENTS</b> . . . . .	vi
<b>CONTENTS</b> . . . . .	vii
<b>LIST OF TABLES</b> . . . . .	ix
<b>LIST OF FIGURES</b> . . . . .	x
<b>CHAPTER</b>	
<b>1 INTRODUCTION</b> . . . . .	<b>1</b>
<b>2 BACKGROUND KNOWLEDGE</b> . . . . .	<b>4</b>
2.1 Introduction to SDEs . . . . .	4
2.2 Numerical methods for SDEs . . . . .	8
2.3 SDEs models . . . . .	9
2.3.1 Brownian motion on a sphere . . . . .	9
2.3.2 SDEs whose solutions move toward a particular point . . . . .	10
2.4 Introduction to map projections . . . . .	10
2.4.1 Latitude and longitude . . . . .	10
2.4.2 Map projections . . . . .	11
<b>3 METHOD</b> . . . . .	<b>18</b>
3.1 Understanding of animal migration cycle . . . . .	18
3.2 Setting of animal migration model . . . . .	19
3.2.1 Time domain and pattern . . . . .	19
3.2.2 Criterion of selecting map projection . . . . .	19
3.3 Construction of numerical schemes . . . . .	20
<b>4 RESULTS</b> . . . . .	<b>26</b>
4.1 Sardine run . . . . .	26
4.2 Wildebeest migration . . . . .	33
4.3 Arctic tern migration . . . . .	41
<b>5 CONCLUSION AND FUTURE WORK</b> . . . . .	<b>52</b>

CHAPTER	Page
REFERENCES . . . . .	55
APPENDICES . . . . .	57
BIOGRAPHY . . . . .	62





## LIST OF TABLES

Table	Page
4.1 The coordinates of representative locations. . . . .	34
4.2 The 4 patterns of wildebeest migration and their probabilities. . . . .	35
4.3 The coordinates of representative locations. . . . .	43
4.4 The 10 patterns of arctic tern migration and their probabilities. . . . .	44
1 Parameters $\gamma_n$ and $\sigma_n$ for sardine run migration model. . . . .	58
2 Parameter $\gamma_n$ for wildebeest migration model. . . . .	58
3 Parameter $\sigma_n$ for wildebeest migration model. . . . .	59
4 Parameter $\gamma_n$ for arctic tern migration model. . . . .	60
5 Parameter $\sigma_n$ for arctic tern migration model. . . . .	61



## LIST OF FIGURES

Figure	Page
2.1 The Tissot's indicatrices are circles of identical true radius on the Earth's surface. . . . .	12
2.2 The STER projection is shown centered at $(\phi_0, \theta_0) = (0^\circ, 0^\circ)$ . . . . .	13
2.3 The TMER projection is shown centered at Greenwich with $(\phi_0, \theta_0) = (0^\circ, 0^\circ)$ . . . . .	14
2.4 The LCC projection is shown with standard parallels on the northern hemisphere with $(\phi_0, \theta_0) = (45^\circ, 0^\circ)$ , $\phi_1 = 15^\circ$ and $\phi_2 = 75^\circ$ . . . . .	15
3.1 Time domain with their probabilities and representative points for each periods. . . . .	19
3.2 Time domain for simulation on $[t_{n-1}, t_n]$ . . . . .	25
4.1 Map of the South Coast of South Africa with the path of the sea currents [15]. . . . .	27
4.2 The discretized time of migration routes of sardine run. . . . .	28
4.3 Coordinate $(\phi, \theta)$ of simulation of the routes of sardine run modeled on the sphere. . . . .	29
4.4 Coordinate $(\phi, \theta)$ of simulation of the routes of sardine run modeled on the plane. . . . .	29
4.5 The Q-Q plots of processes on the plane and the sphere. . . . .	30
4.6 Latitude movement of 100 sardines modeled on the sphere. . . . .	30
4.7 Latitude movement of 100 sardines modeled on the plane. . . . .	31
4.8 Longitude movement of 100 sardines modeled on the sphere. . . . .	31
4.9 Longitude movement of 100 sardines modeled on the plane. . . . .	32
4.10 Simulation of sardine run routes displayed on the sphere. . . . .	32
4.11 Map of wildebeest migration routes with monthly behaviors [16]. . . . .	33
4.12 The routes of wildebeest migration for each period. . . . .	36
4.13 Coordinate $(\phi, \theta)$ of simulation of wildebeest migration routes modeled on the sphere. . . . .	37
4.14 Coordinate $(\phi, \theta)$ of simulation of wildebeest migration routes modeled on the plane. . . . .	37
4.15 The Q-Q plots of processes on the plane and the sphere. . . . .	38
4.16 Latitude movement of 100 wildebeests modeled on the sphere. . . . .	39

4.17	Latitude movement of 100 wildebeests modeled on the plane. . . . .	39
4.18	Longitude movement of 100 wildebeests modeled on the sphere. . . . .	40
4.19	Longitude movement of 100 wildebeests modeled on the plane. . . . .	40
4.20	Simulation of wildebeest migration routes displayed on the sphere. . . . .	41
4.21	Southbound migration routes of arctic terns. . . . .	42
4.22	Northbound migration routes of arctic terns. . . . .	42
4.23	The routes of arctic tern migration for each period. . . . .	46
4.24	Coordinate $(\phi, \theta)$ of simulation of the routes of arctic tern migration on the sphere. . . . .	47
4.25	Coordinate $(\phi, \theta)$ of simulation of the routes of arctic tern migration on the plane. . . . .	47
4.26	The Q-Q plots of processes on the plane and the sphere. . . . .	48
4.27	Latitude movement of 100 arctic terns modeled on the sphere. . . . .	49
4.28	Latitude movement of 100 arctic terns modeled on the plane. . . . .	49
4.29	Longitude movement of 100 arctic terns modeled on the sphere. . . . .	50
4.30	Longitude movement of 100 arctic terns modeled on the plane. . . . .	50
4.31	Simulation of arctic tern migration routes displayed on the sphere. . . . .	51

# CHAPTER I

## INTRODUCTION

Animal migration is a fabulous phenomenon in nature of movement of animals from one place to other places according to seasonal conditions. A migration cycle is often annually and closely linked with the cyclic pattern of the seasons.

In the last decades, an understanding of animal migration has been developed continuously, but the ultimate cause is still obscure. Animal migration models have been constructed to predict the movement and plenty of empirical data have been collected to illustrate migration routes to describe patterns of migration. However, in most of results in literature [1, 2, 3], the number of complete records for round-trip tracking is low due to limited funds and lost of signals and tags.

In general, a short-distance migration is modeled mathematically on a planar surface, but most animals have a long-distance migration, e.g., arctic terns migrate from the North Pole to the South Pole [4]; thus, their migration should be modeled on a spherical surface. Additionally, the Brownian motion term is included in a model to represent the existence of noises and randomness of movements. In 1949, the system of stochastic differential equations (SDEs) for the Brownian motion on a sphere was proposed by Yosida [5] in the form

$$d\phi_t = \hat{\sigma} dU_t + \frac{\hat{\sigma}^2}{2 \tan \phi_t} dt, \quad (1.1)$$

$$d\theta_t = \frac{\hat{\sigma}}{\sin \phi_t} dV_t, \quad (1.2)$$

where  $\phi_t$  and  $\theta_t$  represent the latitude and longitude coordinates of a Brownian particle at time  $t$ , respectively, where  $0 \leq \phi_t \leq \pi$  and  $0 \leq \theta_t \leq 2\pi$ ,  $\hat{\sigma}^2$  is a variance parameter, and  $U_t$  and  $V_t$  are independent standard Brownian motions. In 1986,

Le Gall and Yor [6] worked with a diffusion on a sphere with general drift terms by adding some drifts to the Yosida's model (1.1)-(1.2) to have the form

$$d\phi_t = \hat{\sigma} dU_t + \frac{\hat{\sigma}^2}{2 \tan \phi_t} dt + f(\phi_t, \theta_t) dt, \quad (1.3)$$

$$d\theta_t = \frac{\hat{\sigma}}{\sin \phi_t} dV_t + g(\phi_t, \theta_t) dt, \quad (1.4)$$

where  $f$  and  $g$  are bounded measurable functions on  $[0, \pi] \times \mathbb{R}/2\pi\mathbb{Z}$ . In 1998, Bellinger and Stewart [7] applied this model (1.3)-(1.4) to the migration of elephant-seals that migrate directly towards the North Pole by adding an appropriate speed constant ( $\delta$ ) to the drift term to have the form

$$d\phi_t = \hat{\sigma} dU_t + \left( \frac{\hat{\sigma}^2}{2 \tan \phi_t} - \delta \right) dt, \quad (1.5)$$

$$d\theta_t = \frac{\hat{\sigma}}{\sin \phi_t} dV_t. \quad (1.6)$$

In this work, we describe the movement of a point  $(X_t, Y_t)$  toward a point  $(X^*, Y^*)$  by using SDEs which is given by [8]

$$dX_t = \frac{-\gamma(X_t - X^*)}{(X_t - X^*)^2 + (Y_t - Y^*)^2} dt + \sigma dU_t, \quad (1.7)$$

$$dY_t = \frac{-\gamma(Y_t - Y^*)}{(X_t - X^*)^2 + (Y_t - Y^*)^2} dt + \sigma dV_t, \quad (1.8)$$

where  $\gamma$  represents the speed of movement,  $\sigma^2$  is a variance parameter, and  $U_t$  and  $V_t$  are independent standard Brownian motions.

The aim of this work is to establish animal migration models by using SDEs together with behavior functions to describe the migration behaviors during their migrations. The models are developed based on the transformation between SDEs (1.7)-(1.8) on a plane and SDEs (1.1)-(1.2) by using different behavior functions, namely map projections.

Let  $[0, T]$  be the time domain for a cycle of particular animal migration hav-

ing  $N$  sub-intervals of times corresponding to  $N$  behaviors during the migration. We discretize the interval  $[0, T]$  into  $N$  periods, namely  $[t_{n-1}, t_n]$ , for each particular movement behavior, where  $0 = t_0 < t_1 < t_2 < \dots < t_N = T$ . For each particular period  $[t_{n-1}, t_n]$ , the coordinate  $(\phi_t, \theta_t)$  on the sphere is described via an appropriate map projection to transform  $(\phi_t, \theta_t)$  into  $(X_t, Y_t)$  on the plane. The behavior of  $(X_t, Y_t)$  is then modeled based on SDEs (1.7)-(1.8), whose solution moves toward  $(X_n, Y_n)$ , i.e., the transformation of  $(\phi_{t_n}, \theta_{t_n})$  on the sphere.

A system of the SDEs on  $(\phi_t, \theta_t)$  is obtained by applying Itô's Lemma with an appropriate map projection to transform the process from the rectangular coordinates  $(X_t, Y_t)$  into the spherical coordinate  $(\phi_t, \theta_t) \in [0, \pi] \times \mathbb{R}/2\pi\mathbb{Z}$  and adding the drift and diffusion terms based on Yosida's model (1.1) and (1.2). After that, all periods are combined together to display animal migration models via the Euler-Maruyama scheme.

Nevertheless, migrants do not only migrate from one place to another directly, but they also migrate sinuously from one place to another or meander around some targeted areas. Thus, we provide a probability of the different patterns of animal migration to make the models realistic.

The organization of the thesis is given as follows. Background knowledge is described in chapter 2. The methods of modeling animal migrations are presented in chapter 3, and some simulation examples are shown in chapter 4. Finally, in chapter 5, we conclude our work, provide some discussions, and suggest some related future works.

# CHAPTER II

## BACKGROUND KNOWLEDGE

In this chapter, we first introduce SDEs and numerical methods for SDEs which are addressed in [9]. Next, Brownian motion on a sphere [5] and the SDEs whose solutions move toward a particular point [8] are presented. Finally, the basic idea of map projection [10, 11] is provided to describe behavior functions for the model.

### 2.1 Introduction to SDEs

#### Definition 2.1.1. (Stochastic Process)

Let  $I$  be a subset of  $\mathbb{R}$ . A family of random variables  $\{X_t\}_{t \in I}$ , indexed by  $I$ , is called a **stochastic process**.

**Remark :** In most applications, the variable  $t$  stands for time and  $I$  is usually assumed to be a subset of  $[0, \infty)$ .

#### Definition 2.1.2. (Continuous Sample Paths)

Let  $\{X_t\}_{t \in I}$ , be a stochastic process defined on a probability space  $(\Omega, \mathcal{F}, P)$ . For a fixed  $\omega \in \Omega$ , a function  $X_t(\omega): I \rightarrow \mathbb{R}$  is called a **sample path**. The process  $\{X_t\}_{t \in I}$  is said to have **continuous sample paths**, if for almost all  $\omega \in \Omega$ ,  $X_t(\omega)$  is a continuous function on  $I$ .

#### Definition 2.1.3. (Standard Brownian Motion)

A scalar **standard Brownian motion**, or standard **Wiener process**, over  $[0, T]$  is a stochastic process  $\{W_t\}_{t \in [0, T]}$  that satisfies the following four conditions.

1.  $W_0 = 0$  (with probability 1).
2. For  $0 \leq s < t \leq T$ ,  $W_t - W_s$  is normally distributed with mean zero and variance  $t-s$ , i.e.,  $W_t - W_s \sim \mathcal{N}(0, t-s)$ , where  $\mathcal{N}(\mu, \sigma)$  denotes a normally

distributed random variable with mean  $\mu$  and variance  $\sigma$ .

3. For  $0 \leq s < t \leq u < v \leq T$ , the increments  $W_t - W_s$  and  $W_v - W_u$  are independent.
4.  $\{W_t\}_{t \in [0, T]}$  has continuous sample paths.

**Definition 2.1.4. ( $m$ -dimensional Standard Brownian Motion)**

Let  $W_t^{(1)}, W_t^{(2)}, \dots, W_t^{(m)}$  be independent standard Brownian motions.

Then,  $\left\{ \mathbf{W}_t = \left( W_t^{(1)}, W_t^{(2)}, \dots, W_t^{(m)} \right) \right\}_{t \in [0, T]}$  is called an  **$m$ -dimensional standard Brownian motion**.

**Stochastic differential equations** (SDEs) studied in this work are typically of the form

$$dX_t = a(t, X_t)dt + b(t, X_t)dW_t, \quad X_0 = x \quad (2.1)$$

where  $a$  and  $b$  are real-valued functions,  $\{W_t\}_{t \in [0, T]}$  is a standard Brownian motion and  $x \in \mathbb{R}$ . The equation (2.1) is a shorthand notation which should be understood as the stochastic integral equation

$$X_t = X_0 + \int_0^t a(s, X_s)ds + \int_0^t b(s, X_s)dW_s.$$

The integral  $\int_0^t a(s, X_s)ds$  is interpreted in the Riemann sense and the integral  $\int_0^t b(s, X_s)dW_s$  is interpreted in the Itô sense.

For  $n$ -dimensional SDEs,

$$\begin{aligned} dX_t^{(1)} &= a_1(t, \mathbf{X}_t)dt + b_{11}(t, \mathbf{X}_t)dW_t^{(1)} + \dots + b_{1m}(t, \mathbf{X}_t)dW_t^{(m)}, \\ &\vdots \\ dX_t^{(n)} &= a_n(t, \mathbf{X}_t)dt + b_{n1}(t, \mathbf{X}_t)dW_t^{(1)} + \dots + b_{nm}(t, \mathbf{X}_t)dW_t^{(m)}, \end{aligned}$$



where  $\mathbf{X}_t = (X_t^{(1)}, X_t^{(2)}, \dots, X_t^{(n)})$ ,  $a_i$  and  $b_{ij}$  are real-valued functions for  $i = 1, 2, \dots, n$  and  $j = 1, 2, \dots, m$  and  $\{\mathbf{W}_t\}_{t \geq 0}$  is an  $m$ -dimensional standard Brownian motion. It can be written in matrix notation as

$$d\mathbf{X}_t = \mathbf{a}(t, \mathbf{X}_t) dt + \mathbf{b}(t, \mathbf{X}_t) d\mathbf{W}_t$$

where

$$d\mathbf{X}_t = \begin{bmatrix} dX_t^{(1)} \\ dX_t^{(2)} \\ \vdots \\ dX_t^{(n)} \end{bmatrix}, \quad d\mathbf{W}_t = \begin{bmatrix} dW_t^{(1)} \\ dW_t^{(2)} \\ \vdots \\ dW_t^{(m)} \end{bmatrix},$$

$$\mathbf{a}(t, \mathbf{X}_t) = \begin{bmatrix} a_1(t, \mathbf{X}_t) \\ a_2(t, \mathbf{X}_t) \\ \vdots \\ a_n(t, \mathbf{X}_t) \end{bmatrix}, \quad \mathbf{b}(t, \mathbf{X}_t) = \begin{bmatrix} b_{11}(t, \mathbf{X}_t) & b_{12}(t, \mathbf{X}_t) & \cdots & b_{1m}(t, \mathbf{X}_t) \\ b_{21}(t, \mathbf{X}_t) & b_{22}(t, \mathbf{X}_t) & \cdots & b_{2m}(t, \mathbf{X}_t) \\ \vdots & \vdots & \ddots & \vdots \\ b_{n1}(t, \mathbf{X}_t) & b_{n2}(t, \mathbf{X}_t) & \cdots & b_{nm}(t, \mathbf{X}_t) \end{bmatrix}.$$

**Definition 2.1.5. (Infinitesimal Generator)**

Let  $\mathbf{X}_t$  be a solution of the SDE  $d\mathbf{X}_t = \mathbf{a}(\mathbf{X}_t) dt + \mathbf{b}(\mathbf{X}_t) d\mathbf{W}_t$ . The **infinitesimal generator**  $A$  of  $\mathbf{X}_t$  is defined by

$$Af(\mathbf{x}) = \lim_{t \rightarrow 0} \frac{\mathbb{E}(f(\mathbf{X}_t) | \mathbf{X}_0 = \mathbf{x}) - f(\mathbf{x})}{t}, \quad \mathbf{x} \in \mathbb{R}^n.$$

The set of functions  $f : \mathbb{R}^n \rightarrow \mathbb{R}$  such that the limit exists at  $\mathbf{x}$  is denoted by  $\mathcal{D}_A(\mathbf{x})$ , while  $\mathcal{D}_A$  denotes the set of functions for which the limit exists for all  $\mathbf{x} \in \mathbb{R}^n$ .

**Theorem 2.1.1.** Let  $\mathbf{X}_t$  be a solution of the SDE  $d\mathbf{X}_t = \mathbf{a}(\mathbf{X}_t) dt + \mathbf{b}(\mathbf{X}_t) d\mathbf{W}_t$

and  $C_0^2(\mathbb{R}^n)$  denotes the set of the continuous functions from  $\mathbb{R}^n$  into  $\mathbb{R}$  with continuous partial derivatives up to order 2 with compact support in  $\mathbb{R}^n$ . If  $f \in C_0^2(\mathbb{R}^n)$ , then  $f \in \mathcal{D}_A$  and the **infinitesimal generator** of the process  $\mathbf{X}_t$  is given by

$$Af(\mathbf{x}) = \sum_{i=1}^n a_i(\mathbf{x}) \frac{\partial f}{\partial x_i}(\mathbf{x}) + \frac{1}{2} \sum_{i=1}^n \sum_{j=1}^n (b(\mathbf{x})b(\mathbf{x})^T)_{i,j} \frac{\partial^2 f}{\partial x_i \partial x_j}(\mathbf{x}), \quad \text{for } \mathbf{x} \in \mathbb{R}^n.$$

**Remark :** Applying Theorem 2.1.1 with  $d\mathbf{X}_t = d\mathbf{W}_t$ , we have  $n = m$ ,  $\mathbf{a}(\mathbf{X}_t) = \mathbf{0}$  and  $\mathbf{b}(\mathbf{X}_t) = I_n$ , the  $n$ -dimensional identity matrix. Thus, the generator of  $\mathbf{W}_t$  is

$$Af(\mathbf{x}) = \frac{1}{2} \sum_{i=1}^n \frac{\partial^2 f(\mathbf{x})}{\partial x_i^2}, \quad \text{for } f \in C_0^2(\mathbb{R}^n).$$

Thus, we have the following corollary.

**Corollary 2.1.1.1.** The infinitesimal generator of  $n$ -dimensional Brownian motion is half of the Laplace operator, i.e.,  $A = \frac{1}{2}\Delta$ .

**Theorem 2.1.2. Itô's Lemma (Multi-dimensional)**

Let  $\mathbf{X}_t$  be a solution of the SDE

$$d\mathbf{X}_t = \mathbf{a}(t, \mathbf{X}_t) dt + \mathbf{b}(t, \mathbf{X}_t) d\mathbf{W}_t.$$

Let  $\mathbf{g}(t, \mathbf{x}) = (g_1(t, \mathbf{x}), \dots, g_p(t, \mathbf{x}))$  be a  $C^2$  map from  $[0, \infty) \times \mathbb{R}^n$  into  $\mathbb{R}^p$ . Then, for  $k = 1, 2, \dots, p$ , the SDE for the process  $Y_t^{(k)} = g_k(t, \mathbf{X}_t)$  is

$$\begin{aligned} dY_t^{(k)} &= \frac{\partial g_k}{\partial t}(t, \mathbf{X}_t) dt + \sum_{i=1}^n \frac{\partial g_k}{\partial x_i}(t, \mathbf{X}_t) dX_t^{(i)} \\ &\quad + \frac{1}{2} \sum_{i=1}^n \sum_{j=1}^n \frac{\partial^2 g_k}{\partial x_i \partial x_j}(t, \mathbf{X}_t) dX_t^{(i)} dX_t^{(j)} \end{aligned}$$

where  $dW_t^{(i)} dW_t^{(j)} = \delta_{ij} dt$ ,  $dW_t^{(i)} dt = dt dW_t^{(i)} = dt dt = 0$  for all  $i, j = 1, 2, \dots, n$ .

## 2.2 Numerical methods for SDEs

Let  $[0, T]$  be the domain that we want to compute the numerical solution of the SDE (2.1). We first discretize the domain  $[0, T]$  into  $N$  equal pieces for some positive integer  $N$  and let  $\Delta t = T/N$ . Next, we define  $\tau_n = n\Delta t$ . Taking integration from  $\tau_{n-1}$  to  $\tau_n$  through (2.1), we have that

$$X_{\tau_n} = X_{\tau_{n-1}} + \int_{\tau_{n-1}}^{\tau_n} a(t, X_t)dt + \int_{\tau_{n-1}}^{\tau_n} b(t, X_t)dW_t,$$

for  $n = 1, 2, \dots, N$ . The simple way to find the numerical solution of  $X_{\tau_n}$  is approximating the integrands evaluating at the left end of the time interval. Thus, we have

$$\begin{aligned} X_{\tau_n} &\approx X_{\tau_{n-1}} + \int_{\tau_{n-1}}^{\tau_n} a(\tau_{n-1}, X_{\tau_{n-1}})dt + \int_{\tau_{n-1}}^{\tau_n} b(\tau_{n-1}, X_{\tau_{n-1}})dW_t \\ &= X_{\tau_{n-1}} + a(\tau_{n-1}, X_{\tau_{n-1}}) \int_{\tau_{n-1}}^{\tau_n} dt + b(\tau_{n-1}, X_{\tau_{n-1}}) \int_{\tau_{n-1}}^{\tau_n} dW_t \\ &= X_{\tau_{n-1}} + a(\tau_{n-1}, X_{\tau_{n-1}})(\tau_n - \tau_{n-1}) + b(\tau_{n-1}, X_{\tau_{n-1}})(W_{\tau_n} - W_{\tau_{n-1}}). \end{aligned}$$

Due to the fact that  $\tau_n - \tau_{n-1} = \Delta t$  for all  $n$  and the property of standard Brownian motion, we have that

$$X_{\tau_n} \approx X_{\tau_{n-1}} + a(\tau_{n-1}, X_{\tau_{n-1}})\Delta t + b(\tau_{n-1}, X_{\tau_{n-1}})\Delta W_n,$$

where  $\Delta W_n \stackrel{\text{iid}}{\sim} \mathcal{N}(0, \Delta t)$ .

Let  $x_n$  be the numerical solution of  $X_{\tau_n}$ , then the Euler-Maruyama method for (2.1) is given by  $x_0 = x$  and

$$x_n = x_{n-1} + a(\tau_{n-1}, x_{n-1})\Delta t + b(\tau_{n-1}, x_{n-1})\Delta W_n \quad (2.2)$$

for  $n = 1, 2, \dots, N$ , where  $\Delta W_n \stackrel{\text{iid}}{\sim} \mathcal{N}(0, \Delta t)$ .

Similarly, for applying numerical method to  $m$ -dimensional SDEs, we can compute the numerical solution in each dimension with particular numerical scheme.

## 2.3 SDEs models

### 2.3.1 Brownian motion on a sphere

In 1949, Yosida gives the system of SDEs for the Brownian motion on a sphere

$$d\phi_t = \hat{\sigma} dU_t + \frac{\hat{\sigma}^2}{2 \tan \phi_t} dt, \quad (1.1)$$

$$d\theta_t = \frac{\hat{\sigma}}{\sin \phi_t} dV_t, \quad (1.2)$$

where  $\phi_t$  and  $\theta_t$  represent the latitude and longitude of a Brownian particle on a sphere at time  $t$ , respectively, such that  $0 \leq \phi_t \leq \pi$  and  $0 \leq \theta_t < 2\pi$ ,  $\sigma^2$  is a variance parameter, and  $U_t$  and  $V_t$  are independent standard Brownian motions.

According to Corollary 2.1.1.1, we know that the infinitesimal generator of  $n$ -dimensional Brownian motion is half of the Laplace operator. Here, we will show that  $(\phi_t, \theta_t)$  in the Yosida's model is a Brownian motion on a sphere, i.e., the infinitesimal generator of the Yosida's model is the multiple of the spherical Laplacian  $\Delta^*$  which is given by [12],

$$\Delta^* = \frac{1}{\tan \phi} \frac{\partial}{\partial \phi} + \frac{\partial^2}{\partial \phi^2} + \frac{1}{\sin^2 \phi} \frac{\partial^2}{\partial \theta^2}.$$

From Theorem 2.1.1, the infinitesimal generator of  $(\phi_t, \theta_t)^T$  in (1.1) and (1.2) is

$$\begin{aligned} G &= \frac{\sigma^2}{2 \tan \phi} \frac{\partial}{\partial \phi} + \frac{\sigma^2}{2} \frac{\partial^2}{\partial \phi^2} + \frac{\sigma^2}{2 \sin^2 \phi} \frac{\partial^2}{\partial \theta^2} \\ &= \frac{\sigma^2}{2} \left( \frac{1}{\tan \phi} \frac{\partial}{\partial \phi} + \frac{\partial^2}{\partial \phi^2} + \frac{1}{\sin^2 \phi} \frac{\partial^2}{\partial \theta^2} \right) \end{aligned}$$

$$= \frac{\sigma^2}{2} \Delta^*.$$

Hence, the Yosida's model is a Brownian motion on a sphere.

### 2.3.2 SDEs whose solutions move toward a particular point

In [8], a 2-dimensional SDE whose solution moves toward the point  $(X^*, Y^*) \in \mathbb{R}^2$  has the form

$$dX_t = \frac{-\gamma(X_t - X^*)}{(X_t - X^*)^2 + (Y_t - Y^*)^2} dt + \sigma dU_t, \quad (1.7)$$

$$dY_t = \frac{-\gamma(Y_t - Y^*)}{(X_t - X^*)^2 + (Y_t - Y^*)^2} dt + \sigma dV_t, \quad (1.8)$$

where  $\gamma$  represents a rate of moving toward the point  $(X^*, Y^*)$ ,  $\sigma^2$  is a variance parameter, and  $U_t$  and  $V_t$  are independent standard Brownian motions.

## 2.4 Introduction to map projections

### 2.4.1 Latitude and longitude

To identify the location of points on the Earth, longitude and latitude values are often used to refer to these points. Longitude and latitude are angles measured in degree from the earth's center to a point on the earth's surface. In the spherical system, horizontal lines or East–West lines, are lines of equal latitude, or parallels. Vertical lines, or North–South lines, are lines of equal longitude, or meridians. The line of latitude which is midway between the North and South poles is called the equator having zero latitude. The line of zero longitude is called the prime meridian, and for most geographic coordinate systems, the prime meridian is the longitude that passes through Greenwich, England.

Latitude values are measured relative to the equator and range from  $-90^\circ$  at

the South Pole to  $+90^\circ$  at the North Pole. Longitude values are measured relative to the prime meridian. They range from  $-180^\circ$  when traveling west to  $180^\circ$  when traveling east. For example, if the prime meridian is at Greenwich, then Australia, which is south of the equator and east of Greenwich, has positive longitude values and negative latitude values.

### 2.4.2 Map projections

A map projection is a way to transfer the information from a 3-dimensional surface to a 2-dimensional plane. In this work, a map projection is a way to flatten a globe's surface into a plane. It is well known that it is impossible to show the surface of the Earth accurately on a flat map, which was proven mathematically by Leonhard Euler in 1777. A common example is to imagine peeling an orange and pressing the orange peel flat on a table. It would bulge and break. Representing the Earth's surface in two dimensions causes distortion in the shape, area, distance, and direction of the data. A map projection uses mathematical formulas to relate spherical coordinates on the globe to planar coordinates.

There are many types of projections [10, 11]. Different projections cause different types of distortions. The well-known criterion for visualizing the distortions of a map projection is Tissot's Indicatrix. The idea is to measure the deformation when a circle on a sphere is projected onto a plane. Figure 2.1 shows Tissot's indicatrices on the Earth's surface. The deformation of a circle depends on the type of projection. We can select the projection that has less distortions on the specific area.

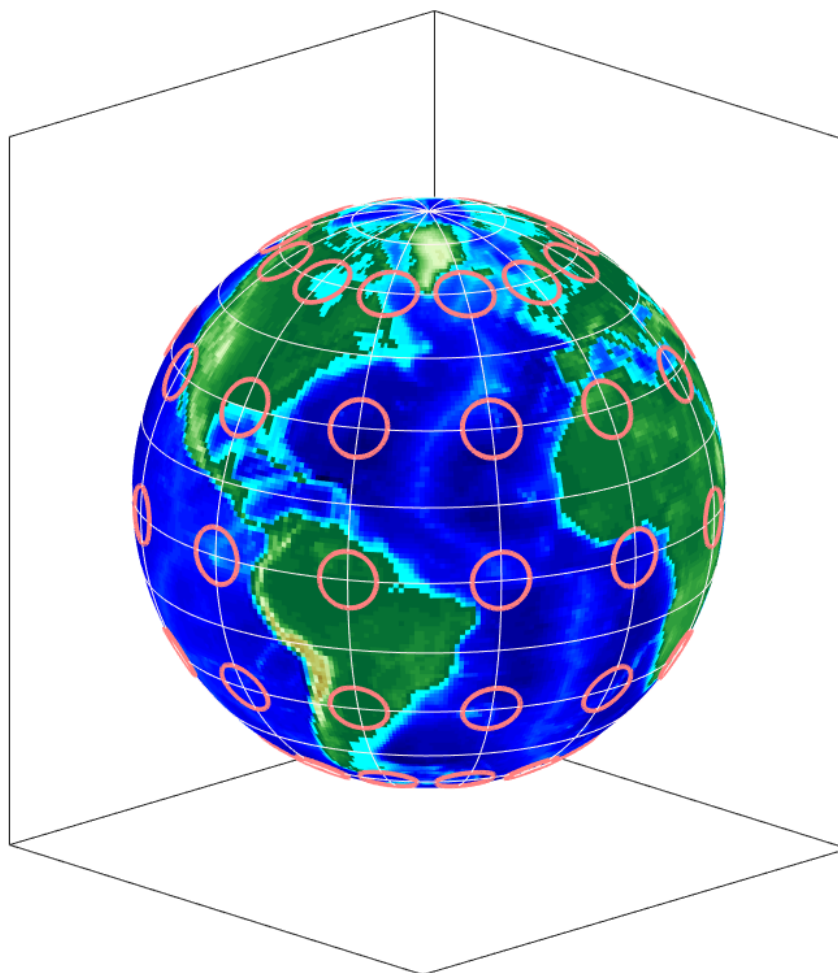
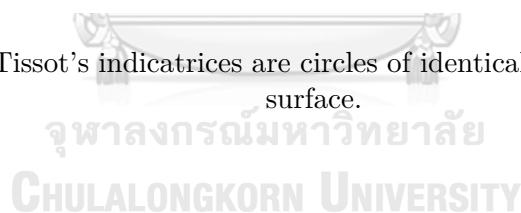


**Figure 2.1:** The Tissot's indicatrices are circles of identical true radius on the Earth's surface.



In this work, we use 3 projections corresponding to 3 behaviors for modeling animal migrations: Stereographic (STER) projection, Transverse Mercator (TMER) projection and Lambert Conformal Conic (LCC) projection.

The STER projection is an appropriate transformation to describe the area around a considered point on the sphere. In our work, it is used to describe movements surrounding the considered area, because the area around a considered point has less distortions. The distortions increase in the area that is far from the considered point. Figure 2.2 shows Tissot's indicatrices transformed by the STER

projection. The farther area from the considered point, the more distortions of the indicatrices.

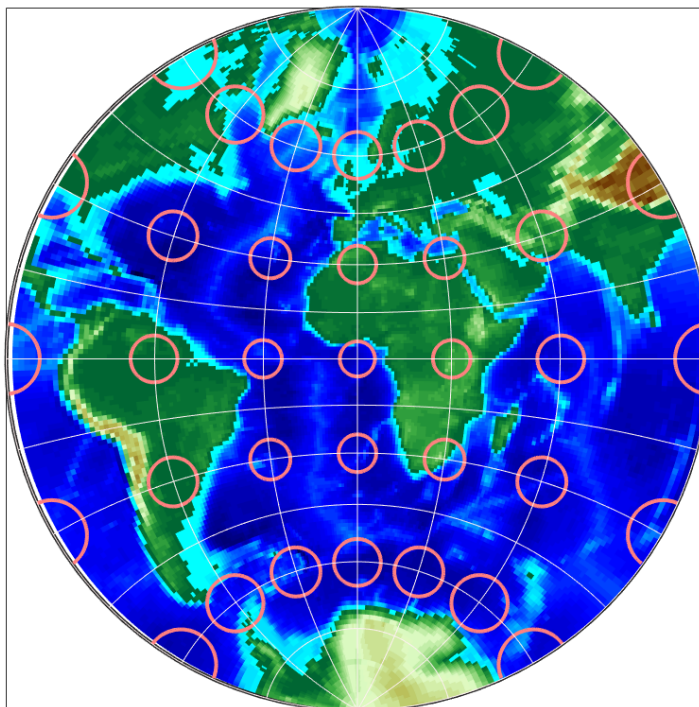


**Figure 2.2:** The STER projection is shown centered at  $(\phi_0, \theta_0) = (0^\circ, 0^\circ)$ .

The TMER projection is preferred for North-South movements which are for movements going North or South directly with low movement in East-West direction. This is because the area near the same longitude of a center point has less distortions. The distortions increase in the area that is far from the longitude of the center point. Figure 2.3 shows Tissot's indicatrices transformed by the TMER projection. The farther the longitude from the center point, the more distortions of the indicatrices.



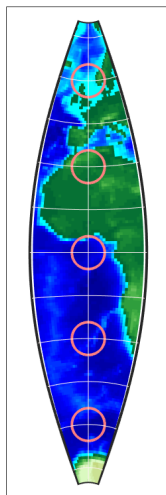


**Figure 2.3:** The TMER projection is shown centered at Greenwich with  $(\phi_0, \theta_0) = (0^\circ, 0^\circ)$ .

The LCC projection is preferred for East-West movements, when the movements are low in the North-South direction. This is because the area near the same latitude of a center point has less distortions. The distortions increase in the area that is far from the latitude of the center point. Figure 2.4 shows Tissot's indicatrices transformed by the LCC projection. The farther the latitude from the center point, the more distortions of the indicatrices.

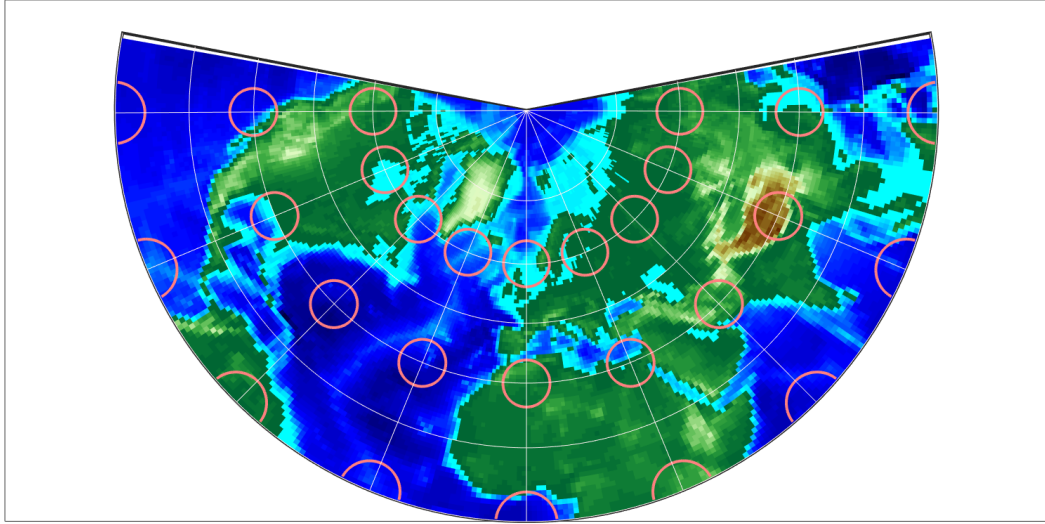


**Figure 2.4:** The LCC projection is shown with standard parallels on the northern hemisphere with  $(\phi_0, \theta_0) = (45^\circ, 0^\circ)$ ,  $\phi_1 = 15^\circ$  and  $\phi_2 = 75^\circ$ .

Let  $(\phi, \theta) \in [-90^\circ, 90^\circ] \times (-180^\circ, 180^\circ]$  be a pair of the latitude and longitude coordinates, respectively, and  $R$  be the radius of the sphere corresponding to the scale of the map.  $(\phi_0, \theta_0)$  is a pair of the latitude and longitude coordinates of the center and  $k_0$  is the scale factor, normally 1.0. Let  $(x, y)$  be a pair of the rectangular coordinates. Note that the Y axis lies along the central meridian  $\theta_0$  with  $y$  increasing northerly, and the X axis is perpendicular through  $\phi_0$  at  $\theta_0$  with  $x$  increasing easterly. The formulas for the 3 projections are given as follows.

**STER projection:**

$$x = R k \cos \phi \sin(\theta - \theta_0), \quad (2.3)$$

$$y = R k [\cos \phi_0 \sin \phi - \sin \phi_0 \cos \phi \cos(\theta - \theta_0)], \quad (2.4)$$

where

$$k = \frac{2k_0}{[1 + \sin \phi_0 \sin \phi + \cos \phi_0 \cos \phi \cos(\theta - \theta_0)]}.$$

For the inverse formulas, given  $R, k_0, \phi_0, \theta_0, x$ , and  $y$ , we have

$$\phi = \arcsin \left( \cos c \sin \phi_0 + \frac{y \sin c \cos \phi_0}{\rho} \right), \quad (2.5)$$

$$\theta = \theta_0 + \arctan \left( \frac{x \sin c}{\rho \cos \phi_0 \cos c - y \sin \phi_0 \sin c} \right), \quad (2.6)$$

where

$$\rho = \sqrt{x^2 + y^2} \quad \text{and} \quad c = 2 \arctan \left( \frac{\rho}{2Rk_0} \right).$$

**TMER projection:**

$$x = \frac{Rk_0}{2} \ln \left( \frac{1+B}{1-B} \right), \quad (2.7)$$

$$y = Rk_0 \left\{ \arctan \left[ \frac{\tan \phi}{\cos(\theta - \theta_0)} \right] - \phi_0 \right\}, \quad (2.8)$$

where

$$B = \cos \phi \sin(\theta - \theta_0).$$

Here, we assume that  $B \neq \pm 1$ .

For the inverse formulas, given  $R, k_0, \phi_0, \theta_0, x$ , and  $y$ , we have

$$\phi = \arcsin \left[ \frac{\sin D}{\cosh\left(\frac{x}{Rk_0}\right)} \right], \quad (2.9)$$

$$\theta = \theta_0 + \arctan \left[ \frac{\sinh\left(\frac{x}{Rk_0}\right)}{\cos D} \right], \quad (2.10)$$

where

$$D = \frac{y}{Rk_0} + \phi_0.$$

**LCC projection:**

$$x = \rho \sin \lambda, \quad (2.11)$$

$$y = \rho_0 - \rho \cos \lambda, \quad (2.12)$$

where

$$\rho = \frac{RF}{\tan^n(\frac{\pi}{4} + \frac{\phi}{2})}, \quad \lambda = n(\theta - \theta_0), \quad \rho_0 = \frac{RF}{\tan^n(\frac{\pi}{4} + \frac{\phi_0}{2})},$$

$$F = \frac{\cos \phi_1 \tan^n(\frac{\pi}{4} + \frac{\phi_1}{2})}{n}, \quad n = \frac{\ln(\frac{\cos \phi_1}{\cos \phi_2})}{\ln \left[ \frac{\tan(\frac{\pi}{4} + \frac{\phi_2}{2})}{\tan(\frac{\pi}{4} + \frac{\phi_1}{2})} \right]},$$

where  $\phi_1$  and  $\phi_2$  are the lower and upper standard latitudes.

For the inverse formulas, given  $R, \phi_1, \phi_2, \phi_0, \theta_0, x$ , and  $y$ , we have

$$\phi = 2 \arctan \sqrt{RF/\hat{\rho}} - \frac{\pi}{2}, \quad (2.13)$$

$$\theta = \hat{\lambda}/n + \theta_0, \quad (2.14)$$

where

$$\hat{\rho} = \text{sign}(n) \sqrt{x^2 + (\rho_0 - y)^2},$$

$$\hat{\lambda} = \arctan \left( \frac{x}{\rho_0 - y} \right).$$

# CHAPTER III

## METHOD

In chapter 3, we present the procedure to establish an animal migration model. In brief, we first research the considered animal migration cycle comprehensively. Then, we discretize the time domain into  $N$  periods which characterize  $N$  different movement behaviors during their migration. We present possible patterns of their migration and provide probabilities for each pattern. For each period, we construct the SDEs whose solution moves toward a particular point on a sphere via Itô's Lemma based on the SDEs whose solution moves toward a particular point on a plane (1.7) and (1.8), with an appropriate map projection formula. We also add the drift and diffusion terms based on Yosida's model (1.1) and (1.2) into the constructed SDEs. All periods are combined together to display animal migration models via the Euler-Maruyama scheme. In detail, this chapter falls into 4 sections as follows.

### 3.1 Understanding of animal migration cycle

First of all, we have to know the main location that they migrate in their migration cycle. What is the time that they depart and arrive for each place? Do they all migrate in the same pattern? How do they move from one place to another? However, all data that we know is incomplete. The understanding of animal migration has been researching for a long time.

## 3.2 Setting of animal migration model

### 3.2.1 Time domain and pattern

**Figure 3.1:** Time domain with their probabilities and representative points for each periods.

We first set time domain  $[t_0, T]$  for simulation. Here,  $t_0$  is a starting time for simulation that we set and  $T$  is a suitable maximum time. Then, we discretize the time domain  $[t_0, T]$  into  $N$  periods, namely  $[t_{n-1}, t_n]$  for  $n = 1, 2, \dots, N$ , corresponding to each particular movement behavior where  $0 = t_0 < t_1 < t_2 < \dots < t_N = T$ . For each  $[t_{n-1}, t_n]$ , we set the fixed point on a sphere to be the representative point  $(\phi_{t_n}, \theta_{t_n})$ , and then, we classify the behavior movement into  $P_n$  possible patterns and provide all probabilities  $p_{n1}, p_{n2}, \dots, p_{nP_n}$  where  $p_{n1} + p_{n2} + \dots + p_{nP_n} = 1$ .

### 3.2.2 Criterion of selecting map projection

According to Section 2.4.2, the STER projection is suitable for transformation on area around a consider point, the TMER projection is suitable for transformation on area near the same longitude of a center point, and the LCC projection is suitable for transformation on area near the same latitude of a center point. Thus, for each period  $[t_{n-1}, t_n]$ , we select an appropriate map projection based on locations of  $(\phi_{t_{n-1}}, \theta_{t_{n-1}})$  and  $(\phi_{t_n}, \theta_{t_n})$  according to the following criteria.

For movement that is not too far away from the point  $(\phi_{t_{n-1}}, \theta_{t_{n-1}})$ , i.e. if  $\sqrt{(\phi_{t_n} - \phi_{t_{n-1}})^2 + (\theta_{t_n} - \theta_{t_{n-1}})^2} < 5^\circ$ , we select the STER projection.

For movement that is far away from the point  $(\phi_{t_{n-1}}, \theta_{t_{n-1}})$ , i.e. if  $\sqrt{(\phi_{t_n} - \phi_{t_{n-1}})^2 + (\theta_{t_n} - \theta_{t_{n-1}})^2} \geq 5^\circ$ , we consider between the variation of latitude and longitude. If the movement goes in the North-South direction more than

East-West direction, i.e.  $|\phi_{t_n} - \phi_{t_{n-1}}| > |\theta_{t_n} - \theta_{t_{n-1}}|$ , we select the TMER projection. If the movement goes in the East-West direction more than North-South direction, i.e.  $|\phi_{t_n} - \phi_{t_{n-1}}| < |\theta_{t_n} - \theta_{t_{n-1}}|$ , we select the LCC projection.

### 3.3 Construction of numerical schemes

In this section, we construct the SDEs whose solution moves toward a point  $(\phi_{t_n}, \theta_{t_n})$  for each period  $[t_{n-1}, t_n]$ . In this work, we model animal migration route both on the plane and the sphere.

For modeling on the plane, for each  $[t_{n-1}, t_n]$ , we use a 2-dimensional SDE whose solution moves toward the point  $(\phi_{t_n}, \theta_{t_n}) \in [-90^\circ, 90^\circ] \times (-180^\circ, 180^\circ]$  which has the form

$$dX_t = \frac{-\gamma_n(X_t - \phi_{t_n})}{(X_t - \phi_{t_n})^2 + (Y_t - \theta_{t_n})^2} dt + \sigma_n dU_t, \quad (3.1)$$

$$dY_t = \frac{-\gamma_n(Y_t - \theta_{t_n})}{(X_t - \phi_{t_n})^2 + (Y_t - \theta_{t_n})^2} dt + \sigma_n dV_t, \quad (3.2)$$

where  $\gamma_n$  represents a rate of moving toward the point  $(\phi_{t_n}, \theta_{t_n})$ , and  $U_t$  and  $V_t$  are independent standard Brownian motions. In this case, the map projections are not required to transform the coordinates between the plane and the sphere.

For modeling on the sphere, we have to transform the SDEs whose solution moves toward a particular point on a sphere via Ito's Lemma based on the SDEs whose solution moves toward a particular point on a plane (1.7) and (1.8), with a suitable selected map projection formula. For each period  $[t_{n-1}, t_n]$ , we set the fixed point on a sphere to be the representative point  $(\phi_{t_n}, \theta_{t_n})$  for  $n = 1, 2, \dots, N$ . The SDEs whose solution moves toward a particular point  $(\phi_{t_n}, \theta_{t_n})$  are based on the SDEs whose solution moves toward a point  $(X_n, Y_n)$  where  $(X_n, Y_n)$  is a transformation point of  $(\phi_{t_n}, \theta_{t_n})$  with a selected map projection formula.

For each period  $[t_{n-1}, t_n]$ , 2-dimensional SDEs whose solution moves toward a point  $(\phi_{t_n}, \theta_{t_n})$  on a sphere is

$$dX_t = \frac{-\gamma(X_t - F_n^{-1}(\phi_{t_n}, \theta_{t_n}))}{(X_t - F_n^{-1}(\phi_{t_n}, \theta_{t_n}))^2 + (Y_t - G_n^{-1}(\phi_{t_n}, \theta_{t_n}))^2} dt + \sigma dU_t, \quad (3.3)$$

$$dY_t = \frac{-\gamma(Y_t - G_n^{-1}(\phi_{t_n}, \theta_{t_n}))}{(X_t - F_n^{-1}(\phi_{t_n}, \theta_{t_n}))^2 + (Y_t - G_n^{-1}(\phi_{t_n}, \theta_{t_n}))^2} dt + \sigma dV_t, \quad (3.4)$$

where  $F_n^{-1}$  and  $G_n^{-1}$  are the selected map projection formulas for the point  $X_n$  and  $Y_n$  in terms of  $(\phi_{t_n}, \theta_{t_n})$ , respectively. From now on, we denote

$$a(X_t, Y_t, \phi_{t_n}, \theta_{t_n}) := \frac{-\gamma(X_t - F_n^{-1}(\phi_{t_n}, \theta_{t_n}))}{(X_t - F_n^{-1}(\phi_{t_n}, \theta_{t_n}))^2 + (Y_t - G_n^{-1}(\phi_{t_n}, \theta_{t_n}))^2},$$

$$b(X_t, Y_t, \phi_{t_n}, \theta_{t_n}) := \frac{-\gamma(Y_t - G_n^{-1}(\phi_{t_n}, \theta_{t_n}))}{(X_t - F_n^{-1}(\phi_{t_n}, \theta_{t_n}))^2 + (Y_t - G_n^{-1}(\phi_{t_n}, \theta_{t_n}))^2}.$$

Thus, (3.3) and (3.4) become

$$dX_t = a(X_t, Y_t, \phi_{t_n}, \theta_{t_n}) dt + \sigma dU_t, \quad (3.5)$$

$$dY_t = b(X_t, Y_t, \phi_{t_n}, \theta_{t_n}) dt + \sigma dV_t. \quad (3.6)$$

Next, we apply Itô's Lemma with the function  $F_n(X, Y)$  and  $G_n(X, Y)$  where  $F_n$  and  $G_n$  are the selected map projection formulas for the point  $\phi_t$  and  $\theta_t$  in terms of  $(X_t, Y_t)$ , respectively. Then, we have

$$d\phi_t = \frac{\partial F_n}{\partial X}(X_t, Y_t) dX_t + \frac{\partial F_n}{\partial Y}(X_t, Y_t) dY_t$$

$$+ \frac{1}{2} \frac{\partial^2 F_n}{\partial X \partial X}(X_t, Y_t) dX_t dX_t + \frac{\partial^2 F_n}{\partial X \partial Y}(X_t, Y_t) dX_t dY_t + \frac{1}{2} \frac{\partial^2 F_n}{\partial Y \partial Y}(X_t, Y_t) dY_t dY_t,$$

$$d\theta_t = \frac{\partial G_n}{\partial X}(X_t, Y_t) dX_t + \frac{\partial G_n}{\partial Y}(X_t, Y_t) dY_t$$

$$+ \frac{1}{2} \frac{\partial^2 G_n}{\partial X \partial X}(X_t, Y_t) dX_t dX_t + \frac{\partial^2 G_n}{\partial X \partial Y}(X_t, Y_t) dX_t dY_t + \frac{1}{2} \frac{\partial^2 G_n}{\partial Y \partial Y}(X_t, Y_t) dY_t dY_t.$$



Replace  $dX_t$  and  $dY_t$  with (3.5) and (3.6) respectively. Then, we have

$$\begin{aligned}
d\phi_t &= \frac{\partial F_n}{\partial X}(X_t, Y_t) (a(X_t, Y_t, \phi_{t_n}, \theta_{t_n}) dt + \sigma dU_t) \\
&\quad + \frac{\partial F_n}{\partial Y}(X_t, Y_t) (b(X_t, Y_t, \phi_{t_n}, \theta_{t_n}) dt + \sigma dV_t) \\
&\quad + \frac{1}{2} \frac{\partial^2 F_n}{\partial X \partial X}(X_t, Y_t) (a(X_t, Y_t, \phi_{t_n}, \theta_{t_n}) dt + \sigma dU_t)^2 \\
&\quad + \frac{\partial^2 F_n}{\partial X \partial Y}(X_t, Y_t) (a(X_t, Y_t, \phi_{t_n}, \theta_{t_n}) dt + \sigma dU_t) (b(X_t, Y_t, \phi_{t_n}, \theta_{t_n}) dt + \sigma dV_t) \\
&\quad + \frac{1}{2} \frac{\partial^2 F_n}{\partial Y \partial Y}(X_t, Y_t) (b(X_t, Y_t, \phi_{t_n}, \theta_{t_n}) dt + \sigma dV_t)^2. \\
d\theta_t &= \frac{\partial G_n}{\partial X}(X_t, Y_t) (a(X_t, Y_t, \phi_{t_n}, \theta_{t_n}) dt + \sigma dU_t) \\
&\quad + \frac{\partial G_n}{\partial Y}(X_t, Y_t) (b(X_t, Y_t, \phi_{t_n}, \theta_{t_n}) dt + \sigma dV_t) \\
&\quad + \frac{1}{2} \frac{\partial^2 G_n}{\partial X \partial X}(X_t, Y_t) (a(X_t, Y_t, \phi_{t_n}, \theta_{t_n}) dt + \sigma dU_t)^2 \\
&\quad + \frac{\partial^2 G_n}{\partial X \partial Y}(X_t, Y_t) (a(X_t, Y_t, \phi_{t_n}, \theta_{t_n}) dt + \sigma dU_t) (b(X_t, Y_t, \phi_{t_n}, \theta_{t_n}) dt + \sigma dV_t) \\
&\quad + \frac{1}{2} \frac{\partial^2 G_n}{\partial Y \partial Y}(X_t, Y_t) (b(X_t, Y_t, \phi_{t_n}, \theta_{t_n}) dt + \sigma dV_t)^2.
\end{aligned}$$

Therefore, we have

$$\begin{aligned}
d\phi_t &= \frac{\partial F_n}{\partial X}(X_t, Y_t) (a(X_t, Y_t, \phi_{t_n}, \theta_{t_n}) dt + \sigma dU_t) \\
&\quad + \frac{\partial F_n}{\partial Y}(X_t, Y_t) (b(X_t, Y_t, \phi_{t_n}, \theta_{t_n}) dt + \sigma dV_t) \\
&\quad + \frac{1}{2} \sigma^2 \left( \frac{\partial^2 F_n}{\partial X \partial X}(X_t, Y_t) + \frac{\partial^2 F_n}{\partial Y \partial Y}(X_t, Y_t) \right) dt, \\
d\theta_t &= \frac{\partial G_n}{\partial X}(X_t, Y_t) (a(X_t, Y_t, \phi_{t_n}, \theta_{t_n}) dt + \sigma dU_t) \\
&\quad + \frac{\partial G_n}{\partial Y}(X_t, Y_t) (b(X_t, Y_t, \phi_{t_n}, \theta_{t_n}) dt + \sigma dV_t) \\
&\quad + \frac{1}{2} \sigma^2 \left( \frac{\partial^2 G_n}{\partial X \partial X}(X_t, Y_t) + \frac{\partial^2 G_n}{\partial Y \partial Y}(X_t, Y_t) \right) dt.
\end{aligned}$$

Replace  $X_t$  and  $Y_t$  by  $F_n^{-1}(\phi_t, \theta_t)$  and  $G_n^{-1}(\phi_t, \theta_t)$ , respectively, where  $F_n^{-1}$  and  $G_n^{-1}$  are the selected map projection formulas for the point  $X_t$  and  $Y_t$  in terms

of  $(\phi_{t_n}, \theta_{t_n})$ , respectively. Thus, we have

$$\begin{aligned}
d\phi_t &= \frac{\partial F_n}{\partial X}(F_n^{-1}(\phi_t, \theta_t), G_n^{-1}(\phi_t, \theta_t)) (a(F_n^{-1}(\phi_t, \theta_t), G_n^{-1}(\phi_t, \theta_t), \phi_{t_n}, \theta_{t_n}) dt + \sigma dU_t) \\
&\quad + \frac{\partial F_n}{\partial Y}(F_n^{-1}(\phi_t, \theta_t), G_n^{-1}(\phi_t, \theta_t)) (b(F_n^{-1}(\phi_t, \theta_t), G_n^{-1}(\phi_t, \theta_t), \phi_{t_n}, \theta_{t_n}) dt + \sigma dV_t) \\
&\quad + \frac{\sigma^2}{2} \left( \frac{\partial^2 F_n}{\partial X \partial X}(F_n^{-1}(\phi_t, \theta_t), G_n^{-1}(\phi_t, \theta_t)) + \frac{\partial^2 F_n}{\partial Y \partial Y}(F_n^{-1}(\phi_t, \theta_t), G_n^{-1}(\phi_t, \theta_t)) \right) dt, \\
d\theta_t &= \frac{\partial G_n}{\partial X}(F_n^{-1}(\phi_t, \theta_t), G_n^{-1}(\phi_t, \theta_t)) (a(F_n^{-1}(\phi_t, \theta_t), G_n^{-1}(\phi_t, \theta_t), \phi_{t_n}, \theta_{t_n}) dt + \sigma dU_t) \\
&\quad + \frac{\partial G_n}{\partial Y}(F_n^{-1}(\phi_t, \theta_t), G_n^{-1}(\phi_t, \theta_t)) (b(F_n^{-1}(\phi_t, \theta_t), G_n^{-1}(\phi_t, \theta_t), \phi_{t_n}, \theta_{t_n}) dt + \sigma dV_t) \\
&\quad + \frac{\sigma^2}{2} \left( \frac{\partial^2 G_n}{\partial X \partial X}(F_n^{-1}(\phi_t, \theta_t), G_n^{-1}(\phi_t, \theta_t)) + \frac{\partial^2 G_n}{\partial Y \partial Y}(F_n^{-1}(\phi_t, \theta_t), G_n^{-1}(\phi_t, \theta_t)) \right) dt.
\end{aligned}$$

Finally, we add the drift and diffusion terms based on Yosida's model (1.1) and (1.2). Thus, we have

$$\begin{aligned}
d\phi_t &= \frac{\partial F_n}{\partial X}(F_n^{-1}(\phi_t, \theta_t), G_n^{-1}(\phi_t, \theta_t)) (a(F_n^{-1}(\phi_t, \theta_t), G_n^{-1}(\phi_t, \theta_t), \phi_{t_n}, \theta_{t_n}) dt + \sigma dU_t) \\
&\quad + \frac{\partial F_n}{\partial Y}(F_n^{-1}(\phi_t, \theta_t), G_n^{-1}(\phi_t, \theta_t)) (b(F_n^{-1}(\phi_t, \theta_t), G_n^{-1}(\phi_t, \theta_t), \phi_{t_n}, \theta_{t_n}) dt + \sigma dV_t) \\
&\quad + \frac{\sigma^2}{2} \left( \frac{\partial^2 F_n}{\partial X \partial X}(F_n^{-1}(\phi_t, \theta_t), G_n^{-1}(\phi_t, \theta_t)) + \frac{\partial^2 F_n}{\partial Y \partial Y}(F_n^{-1}(\phi_t, \theta_t), G_n^{-1}(\phi_t, \theta_t)) \right) dt \\
&\quad + \hat{\sigma} d\hat{U}_t + \frac{\hat{\sigma}^2}{2 \tan \phi_t} dt, \tag{3.5}
\end{aligned}$$

$$\begin{aligned}
d\theta_t &= \frac{\partial G_n}{\partial X}(F_n^{-1}(\phi_t, \theta_t), G_n^{-1}(\phi_t, \theta_t)) (a(F_n^{-1}(\phi_t, \theta_t), G_n^{-1}(\phi_t, \theta_t), \phi_{t_n}, \theta_{t_n}) dt + \sigma dU_t) \\
&\quad + \frac{\partial G_n}{\partial Y}(F_n^{-1}(\phi_t, \theta_t), G_n^{-1}(\phi_t, \theta_t)) (b(F_n^{-1}(\phi_t, \theta_t), G_n^{-1}(\phi_t, \theta_t), \phi_{t_n}, \theta_{t_n}) dt + \sigma dV_t) \\
&\quad + \frac{\sigma^2}{2} \left( \frac{\partial^2 G_n}{\partial X \partial X}(F_n^{-1}(\phi_t, \theta_t), G_n^{-1}(\phi_t, \theta_t)) + \frac{\partial^2 G_n}{\partial Y \partial Y}(F_n^{-1}(\phi_t, \theta_t), G_n^{-1}(\phi_t, \theta_t)) \right) dt \\
&\quad + \frac{\hat{\sigma}}{\sin \phi_t} d\hat{V}_t, \tag{3.6}
\end{aligned}$$

being the SDEs whose solution moves toward a point  $(\phi_{t_n}, \theta_{t_n})$  on a sphere for  $t \in [t_{n-1}, t_n]$  where  $\hat{\sigma}^2$  is a variance parameter for Brownian motion on a sphere, and  $U_t, V_t, \hat{U}_t$ , and  $\hat{V}_t$  are independent standard Brownian motions.

We denote

$$\begin{aligned}
A(\phi_t, \theta_t) &:= \frac{\partial F_n}{\partial X}(F_n^{-1}(\phi_t, \theta_t), G_n^{-1}(\phi_t, \theta_t)) a(F_n^{-1}(\phi_t, \theta_t), G_n^{-1}(\phi_t, \theta_t), \phi_{t_n}, \theta_{t_n}) \\
&\quad + \frac{\partial F_n}{\partial Y}(F_n^{-1}(\phi_t, \theta_t), G_n^{-1}(\phi_t, \theta_t)) b(F_n^{-1}(\phi_t, \theta_t), G_n^{-1}(\phi_t, \theta_t), \phi_{t_n}, \theta_{t_n}) \\
&\quad + \frac{1}{2}\sigma^2 \left( \frac{\partial^2 F_n}{\partial X \partial X}(F_n^{-1}(\phi_t, \theta_t), G_n^{-1}(\phi_t, \theta_t)) + \frac{\partial^2 F_n}{\partial Y \partial Y}(F_n^{-1}(\phi_t, \theta_t), G_n^{-1}(\phi_t, \theta_t)) \right) \\
&\quad + \frac{\hat{\sigma}^2}{2 \tan \phi_t} \\
B(\phi_t, \theta_t) &:= \sigma \frac{\partial F_n}{\partial X}(F_n^{-1}(\phi_t, \theta_t), G_n^{-1}(\phi_t, \theta_t)) \\
C(\phi_t, \theta_t) &:= \sigma \frac{\partial F_n}{\partial Y}(F_n^{-1}(\phi_t, \theta_t), G_n^{-1}(\phi_t, \theta_t)) \\
D(\phi_t, \theta_t) &:= \frac{\partial G_n}{\partial X}(G_n^{-1}(\phi_t, \theta_t), G_n^{-1}(\phi_t, \theta_t)) a(G_n^{-1}(\phi_t, \theta_t), G_n^{-1}(\phi_t, \theta_t), \phi_{t_n}, \theta_{t_n}) \\
&\quad + \frac{\partial G_n}{\partial Y}(G_n^{-1}(\phi_t, \theta_t), G_n^{-1}(\phi_t, \theta_t)) b(G_n^{-1}(\phi_t, \theta_t), G_n^{-1}(\phi_t, \theta_t), \phi_{t_n}, \theta_{t_n}) \\
&\quad + \frac{1}{2}\sigma^2 \left( \frac{\partial^2 G_n}{\partial X \partial X}(G_n^{-1}(\phi_t, \theta_t), G_n^{-1}(\phi_t, \theta_t)) + \frac{\partial^2 G_n}{\partial Y \partial Y}(G_n^{-1}(\phi_t, \theta_t), G_n^{-1}(\phi_t, \theta_t)) \right) \\
E(\phi_t, \theta_t) &:= \sigma \frac{\partial G_n}{\partial X}(G_n^{-1}(\phi_t, \theta_t), G_n^{-1}(\phi_t, \theta_t)) \\
F(\phi_t, \theta_t) &:= \sigma \frac{\partial G_n}{\partial Y}(G_n^{-1}(\phi_t, \theta_t), G_n^{-1}(\phi_t, \theta_t)) \\
G(\phi_t, \theta_t) &:= \hat{\sigma} \\
H(\phi_t, \theta_t) &:= \frac{\hat{\sigma}}{\sin \phi_t}
\end{aligned}$$

Then, (3.5) and (3.6) become

$$d\phi_t = A(\phi_t, \theta_t) dt + B(\phi_t, \theta_t) dU_t + C(\phi_t, \theta_t) dV_t + G(\phi_t, \theta_t) d\hat{U}_t, \quad (3.7)$$

$$d\theta_t = D(\phi_t, \theta_t) dt + E(\phi_t, \theta_t) dU_t + F(\phi_t, \theta_t) dV_t + H(\phi_t, \theta_t) d\hat{V}_t. \quad (3.8)$$

**Figure 3.2:** Time domain for simulation on  $[t_{n-1}, t_n]$ .

Let  $\Delta t_n = \frac{t_n}{L_n}$  for some positive integer  $L_n$ ,  $\tau_i = i\Delta t_n$ , and  $\phi_i$  and  $\theta_i$  be numerical solutions of  $\phi_{\tau_i}$  and  $\theta_{\tau_i}$  at the time  $\tau_i$ . Then, Euler-Maruyama method

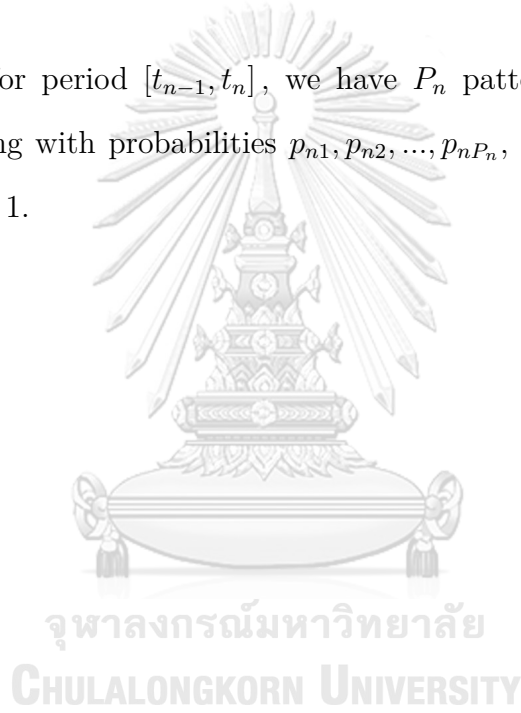
for (3.7) and (3.8) are given by

$$\begin{aligned}\phi_i &= \phi_{i-1} + A(\phi_{i-1}, \theta_{i-1}) \Delta t_n + B(\phi_{i-1}, \theta_{i-1}) \Delta U_i + C(\phi_{i-1}, \theta_{i-1}) \Delta V_i \\ &\quad + G(\phi_{i-1}, \theta_{i-1}) \Delta \hat{U}_i,\end{aligned}\tag{3.9}$$

$$\begin{aligned}\theta_i &= \theta_{i-1} + D(\phi_{i-1}, \theta_{i-1}) \Delta t_n + E(\phi_{i-1}, \theta_{i-1}) \Delta U_i + F(\phi_{i-1}, \theta_{i-1}) \Delta V_i \\ &\quad + H(\phi_{i-1}, \theta_{i-1}) \Delta \hat{V}_i.\end{aligned}\tag{3.10}$$

where  $\Delta U_i, \Delta V_i, \Delta \hat{U}_i, \Delta \hat{V}_i \stackrel{\text{iid}}{\sim} \mathcal{N}(0, \Delta t)$  for  $i = 1, 2, \dots, L_n$ .

Generally, for period  $[t_{n-1}, t_n]$ , we have  $P_n$  patterns. Thus, we have  $P_n$  schemes happening with probabilities  $p_{n1}, p_{n2}, \dots, p_{nP_n}$ , respectively, where  $p_{n1} + p_{n2} + \dots + p_{nP_n} = 1$ .



# CHAPTER IV

## RESULTS

There are many interesting animal migrations around the world, and many of them have not yet been discovered; however, in the last decades, complete migration cycles of some animals have been revealed. In this work, we model and simulate migration routes of 3 animals using SDEs based on observed data in literature. Starting with sardine (*Sardinops sagax*), we display the movement from South Coast of South Africa to the East Coast of South Africa, known as sardine run phenomena. The second migration is wildebeest (*Connochaetes taurinus*), which migrates around Tanzania and Kenya as a complete cycle. The last migration is for arctic tern (*Sterna paradisaea*), which has the longest migration route in the world. The migration of arctic terns routes not only have long distance between Greenland and Antarctica, but also have many patterns. Their migration routes are also showed with complete migration cycles with some possible patterns that we set. The 3 animal migrations are modeled and simulated on the plane and the sphere, which are compared using Q-Q (quantile-quantile) plot.

This chapter is divided into 3 sections corresponding to each considered animal. We provide the behavior movements with suitable parameters (provided in Appendix), and show their migration patterns with the simulations.

### 4.1 Sardine run

Almost every year, the enormous shoal of sardines migrate from the Southern Coast to the Western Coast of Africa. This natural phenomenon is called sardine run. The partial information of sardine run is provided in the references [13, 14].

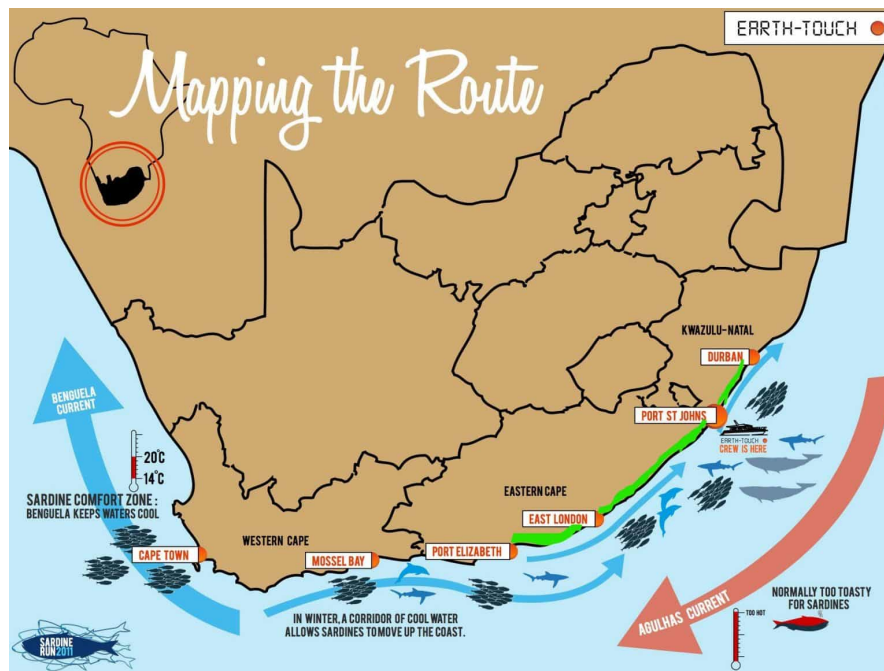


**Figure 4.1:** Map of the South Coast of South Africa with the path of the sea currents [15].

The sardine run does not occur every single year; if it occurs, we will normally see this fantastic phenomenon in late-May to early-June at the South Coast of KwaZulu-Natal, South Africa. Not only we see the huge shoal of sardines, but we also see the predators, such as seabirds, sharks, whales, and dolphins. The full cycle this migration is poorly understood; thus, we partly display their migration routes, from the Southern Coast to the Western Coast of Africa as shown in Figure 4.1.

In this work, we divide the time domain  $[0, T]$  into 3 periods with the representative points as follows:  $AB = \text{Agulhas Bank } (-35^\circ, 21^\circ)$ ;  $T_1$ ,  $T_2$ , and  $T_3 = \text{Transit 1, 2, and 3, with coordinate } (-34.5^\circ, 265^\circ), (-30^\circ, 31.2^\circ), \text{ and } (-29.1^\circ, 32.2^\circ)$ , respectively. For each period, we use the map projections LCC, TMER, and STER to transform the process on the plane to the process on the sphere. The beginning place of simulation is set to be Agulhas Bank and the initial date and time of the



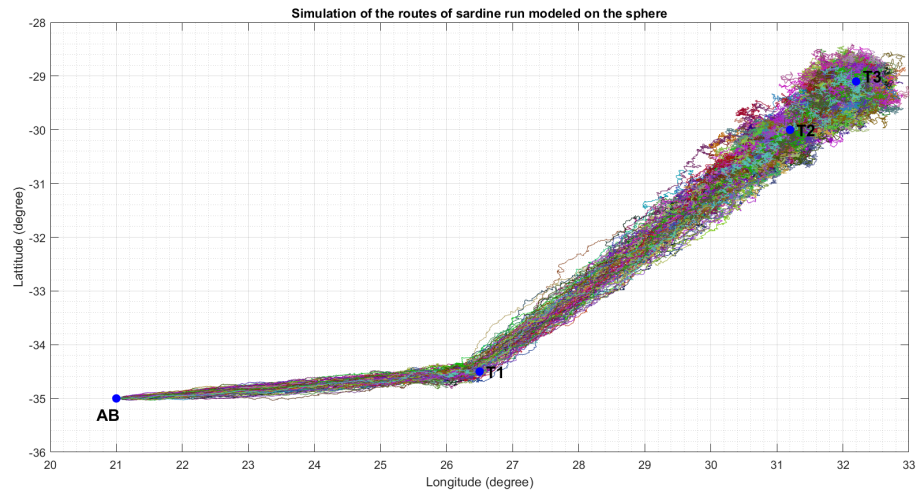


**Figure 4.3:** Coordinate  $(\phi, \theta)$  of simulation of the routes of sardine run modeled on the sphere.

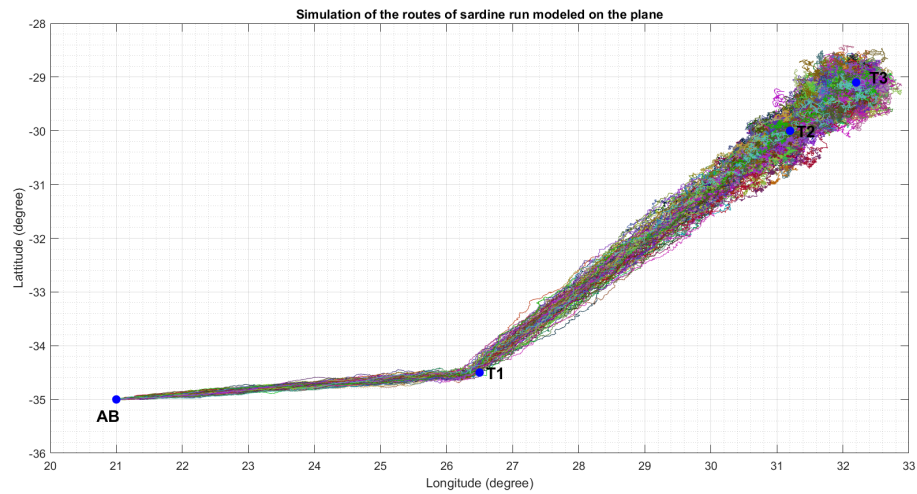


**Figure 4.4:** Coordinate  $(\phi, \theta)$  of simulation of the routes of sardine run modeled on the plane.



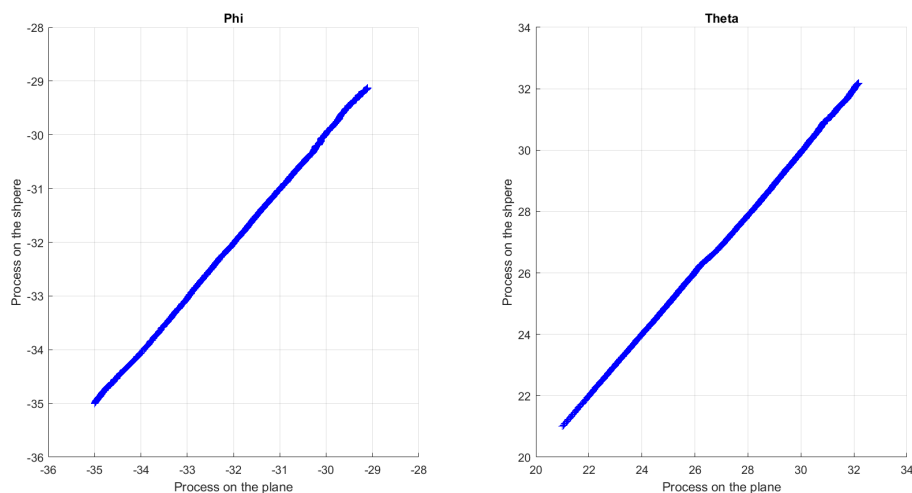


**Figure 4.5:** The Q–Q plots of processes on the plane and the sphere.

Figures 4.3 and 4.4 show the similar results of the simulated coordinates  $(\phi, \theta)$  for both models on the plane and the sphere. First, the 100 sardines depart from AB and go westward to T1, then, they continue to reach T2 and T3, respectively. The simulation accords with their movement. Figure 4.5 shows the distributions between the mean path of the process on the plane and the mean path of the process on the sphere, which are quite similar.

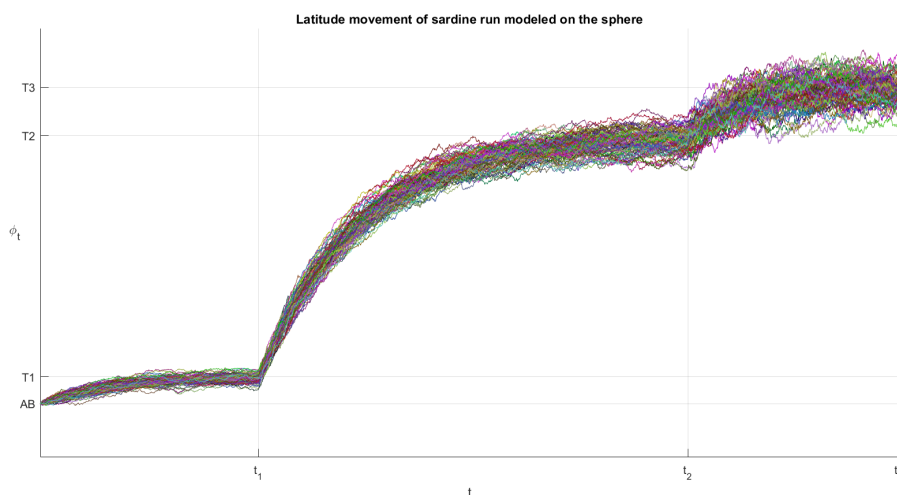


**Figure 4.6:** Latitude movement of 100 sardines modeled on the sphere.

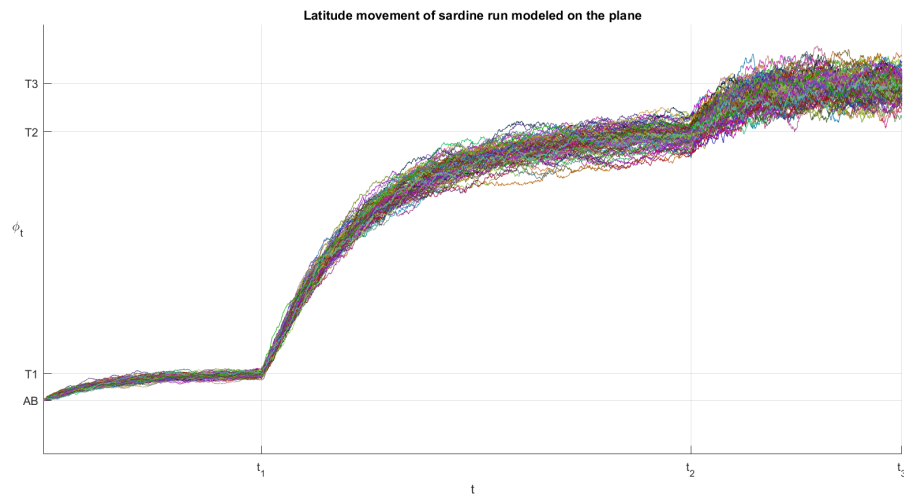


Figure 4.7: Latitude movement of 100 sardines modeled on the plane.

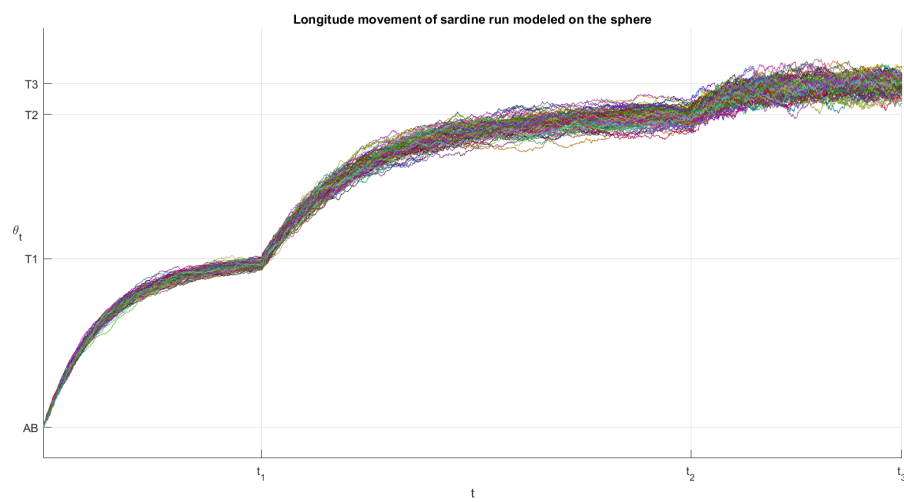
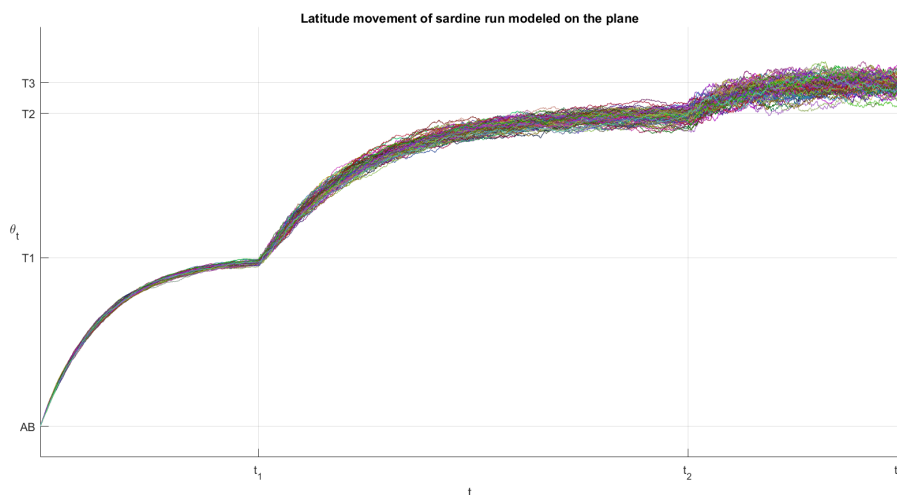
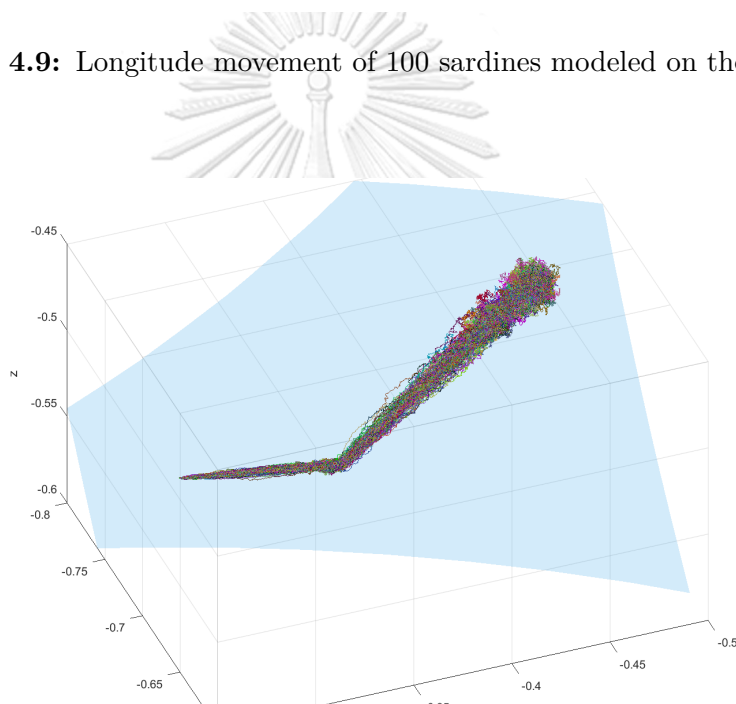


Figure 4.8: Longitude movement of 100 sardines modeled on the sphere.



**Figure 4.9:** Longitude movement of 100 sardines modeled on the plane.



**Figure 4.10:** Simulation of sardine run routes displayed on the sphere.

Figures 4.6 and 4.7 show the latitude movements of 100 sardines during their migration on the sphere and the plane, respectively. The increasing of latitude represents the northward movement. Figures 4.8 and 4.9 show the longitude movements of 100 sardines during their migration on the sphere and the plane, respectively. The increasing of longitude represents the westward movement. Furthermore, the 3-dimension simulation models for sardine run routes on sphere are

shown in Figure 4.10.

## 4.2 Wildebeest migration

One of well-known migrations in Africa is wildebeest migration. Every year, millions of wildebeests have clockwise movement between Tanzania and Kenya, shown in Figure 4.11. They migrate together with zebras, antelopes, gazelles, elands, and impalas. In this work, information of wildebeest migration used in the model is addressed in [16, 17].



**Figure 4.11:** Map of wildebeest migration routes with monthly behaviors [16].

For the modeling and simulation, we set the initial date and time of the migration to be 1<sup>st</sup> January 2008 at noon, and the end date and time to be 1<sup>st</sup> January 2009 at noon, which gives  $T = 480960$  minutes. All representative points are denoted as follows: NCA = Ngorongoro Conservation Area; and T1, T2, T3, T4, T5, T6, T7, T8(1), T8(2), T9 = Transit 1, 2, 3, 4, 5, 6, 7, 8(1), 8(2), 9, respectively, and their coordinates are shown in Table 4.1.

Representative points	Coordinates (degree)
NCA	$(-3^\circ, 35.5^\circ)$
T1	$(-3.43^\circ, 34.9^\circ)$
T2	$(-2.75^\circ, 34.8^\circ)$
T3	$(-2.24^\circ, 34.4^\circ)$
T4	$(-1.87^\circ, 34.2^\circ)$
T5	$(-1.72^\circ, 34.6^\circ)$
T6	$(-1.4^\circ, 34.9^\circ)$
T7	$(-1.56^\circ, 35.1^\circ)$
T8	$(-2.05^\circ, 35.1^\circ)$
T9	$(-2.42^\circ, 35.3^\circ)$

**Table 4.1:** The coordinates of representative locations.

As shown in Figure 4.11 wildebeest migration starts at the Northern part of the Ngorongoro Conservation Area in Tanzania. New wildebeests are born and then move to T1 at the time  $t_1$ . Then, they move upward to T2 and T3 at the time  $t_2$  and  $t_3$ , respectively. Next, at the time  $t_4$ , most herds go to T4 while the others go to  $T_5$ . After that all herds go to T6, T7, and T8 at the time  $t_5$ ,  $t_6$ , and  $t_7$ , respectively. At T8, they continue downward to T9 while some of them stay there before go down to T9. All wildebeests move through T9 and at the time  $t_9$  and go back to NCA at the time  $t_{10}$ .

We assume that there are 4 possible patterns of wildebeest migration. We claim that at the time  $t_4$ , the herds go to T4 and T5 with probabilities  $\frac{3}{4}$  and  $\frac{1}{4}$ , respectively. Also, at the time  $t_7$ , the herds continue downward to T9 and stay at T8 before go down to T9 with probabilities  $\frac{3}{4}$  and  $\frac{1}{4}$ , respectively. The discretized

times and the pathways along with their probabilities of 4 different patterns are shown in Table 4.2.

		Patterns			
n	$t_n$	1	2	3	4
0	0	NCA			
1	43200	T1			
2	64800	T2			
3	192960	T3			
4	217440	T4		T5	
5	260640	T6			
6	325440	T7			
7	358560	T8(1)			
8	427680	T9	T8(2)	T9	T8(2)
9	437760		T9		T9
10	480960	NCA			
Probability		9/16	3/16	3/16	1/16

**Table 4.2:** The 4 patterns of wildebeest migration and their probabilities.

For each pattern  $p$ , let  $0 = t_0 < t_1 < t_2 < \dots < t_{N_p-1} < t_{N_p} = T$ . The period  $[t_{n-1}, t_n]$  represents time interval of different behavior for  $n = 1, 2, \dots, N_p$ . For example, pattern 1 can occur with probability 9/16 that the wildebeests go from NCA to T1, T2, T3, T4, T5, T6, T7, T8 and T9 at the time  $t_1, t_2, t_3, t_4, t_5, t_6, t_7, t_8$  and  $t_9$ , respectively. Finally, they come back to NCA at the time  $t_{10}$ . The other patterns can also be described similarly. The routes of wildebeest migration and the corresponding map projection for each period are shown in Figure 4.12.

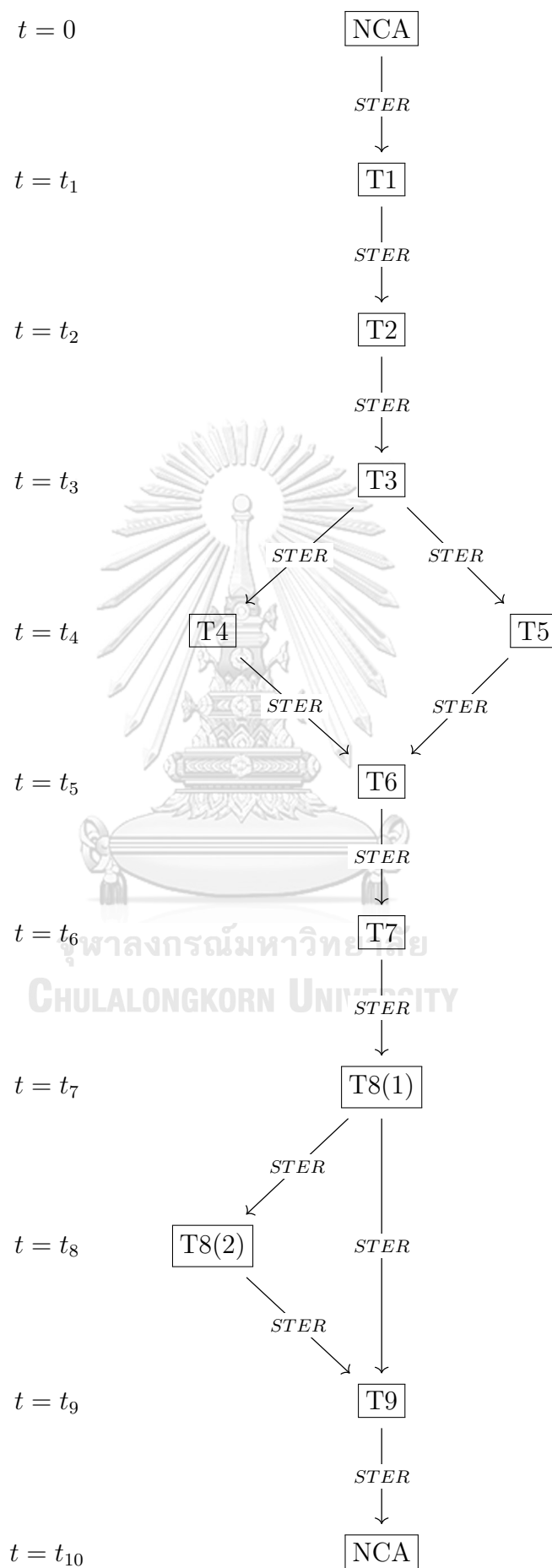


**Figure 4.12:** The routes of wildebeest migration for each period.

The simulated migration routes of 100 wildebeests using  $\Delta t = 60$  with suitable adjusted parameters  $\gamma_n, \sigma_n$  and  $\hat{\sigma}$  (provided in Appendix) for each period, are shown in Figures 4.13 and 4.14.

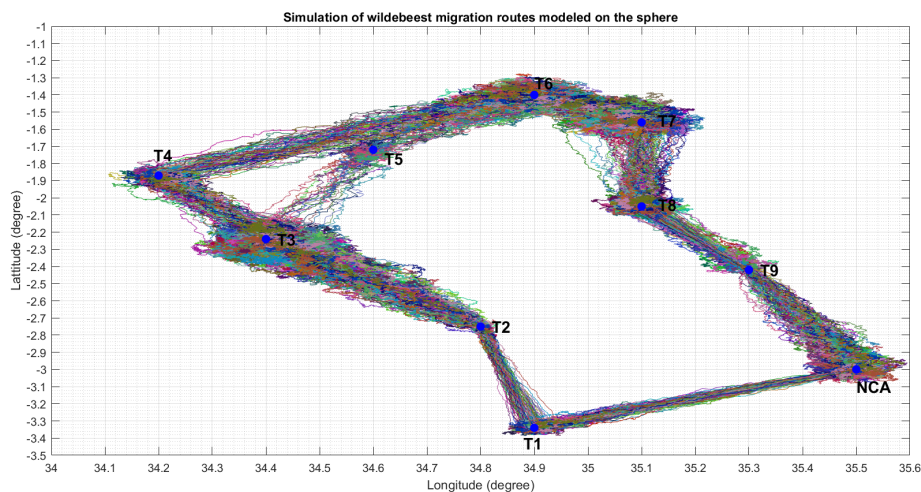


**Figure 4.13:** Coordinate  $(\phi, \theta)$  of simulation of wildebeest migration routes modeled on the sphere.

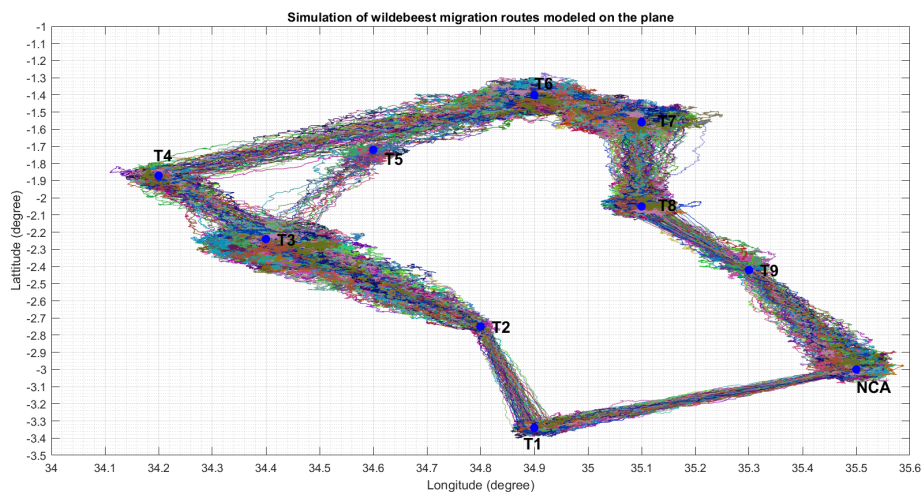


**Figure 4.14:** Coordinate  $(\phi, \theta)$  of simulation of wildebeest migration routes modeled on the plane.



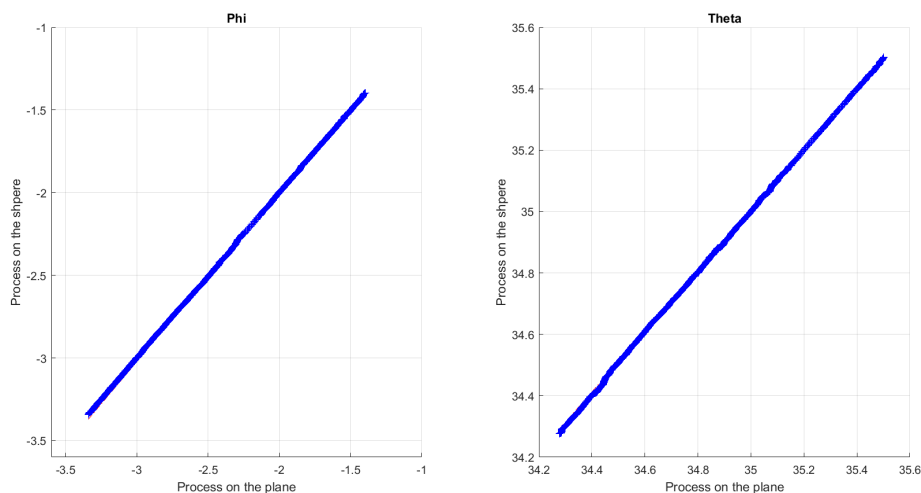


**Figure 4.15:** The Q–Q plots of processes on the plane and the sphere.

Figures 4.13 and 4.14 show the plots of coordinates  $(\phi, \theta)$  of the simulations on the sphere and the plane, respectively, which are quite similar. This shows that wildebeests start from NCA and go to T1, T2, and T3, respectively; at T3, it separate into 2 groups; the one goes to T4 while the other goes to T5; next, they move to T6, T7, and T8, respectively; at T8, some wildebeests stay in this site before go to T9 while the others continue to T9; finally, all wildebeests move to NCA. The simulation results show behaviors as expected according to information in Figure 4.11. Figure 4.15 shows distributions between the mean path of the process on the plane and the mean path of the process on the sphere, which are quite similar.

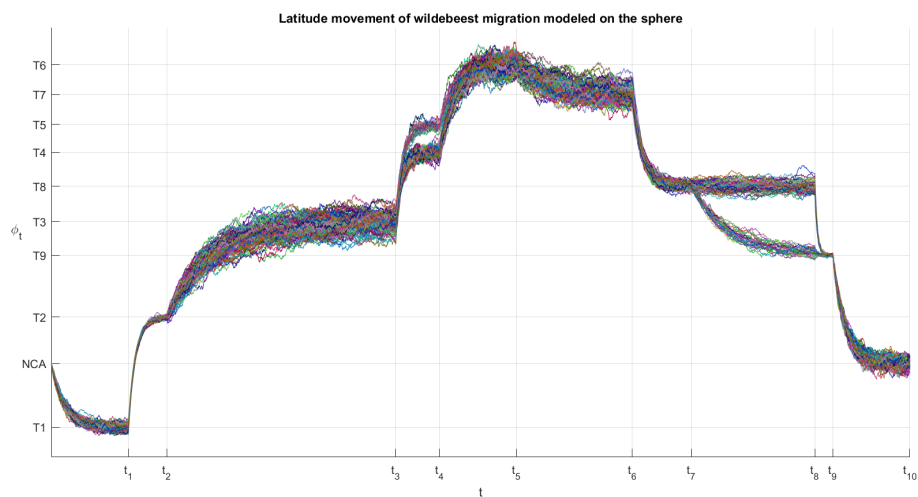


**Figure 4.16:** Latitude movement of 100 wildebeests modeled on the sphere.

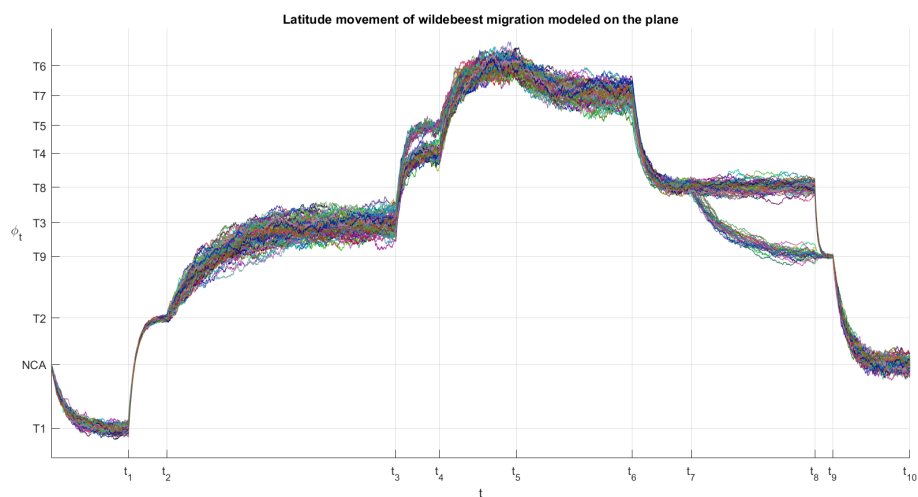


**Figure 4.17:** Latitude movement of 100 wildebeests modeled on the plane.

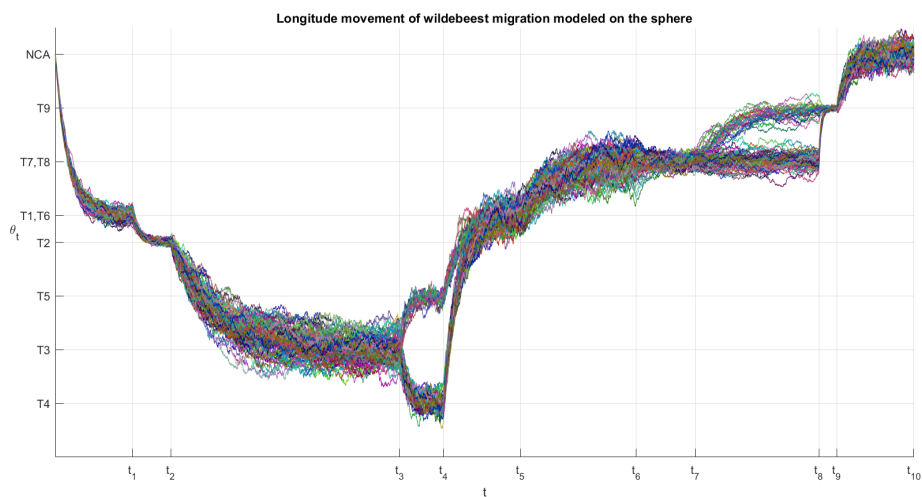


**Figure 4.18:** Longitude movement of 100 wildebeests modeled on the sphere.

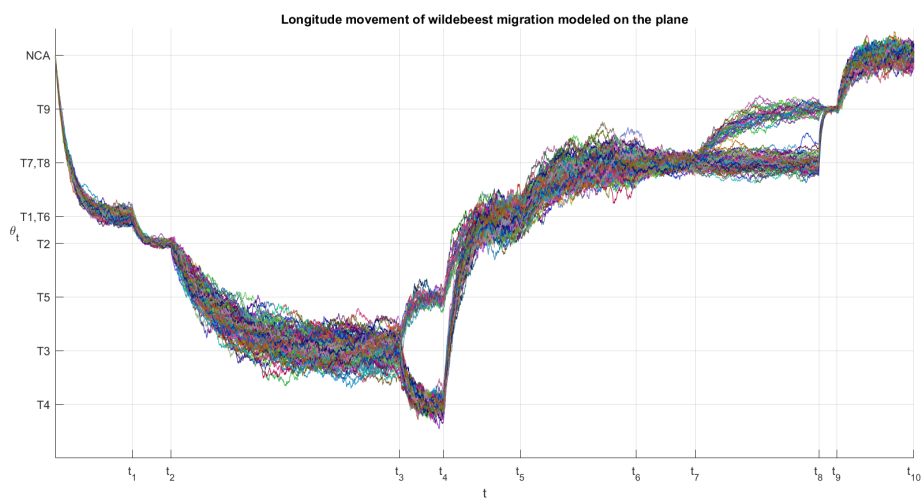


**Figure 4.19:** Longitude movement of 100 wildebeests modeled on the plane.

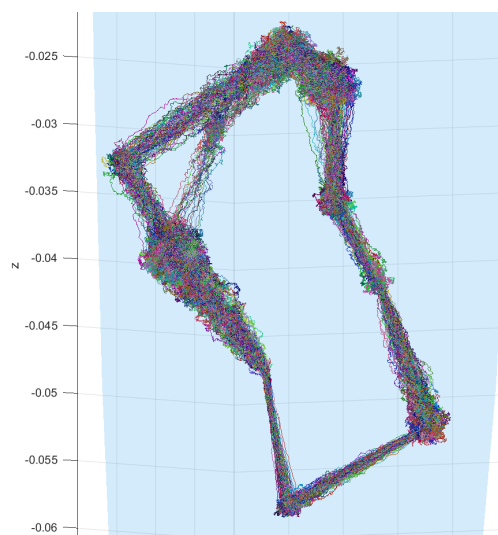


**Figure 4.20:** Simulation of wildebeest migration routes displayed on the sphere.

Figures 4.16 and 4.17 show the latitude movements of 100 wildebeests during their migration on the sphere and the plane, respectively; the increasing of latitude represents the northward movement, while the decreasing of latitude represents the southward movement. Figures 4.18 and 4.19 show the longitude movements of 100 wildebeests during their migration on the sphere and the plane, respectively; the increasing of longitude represent the westward movement, while the decreasing of longitude represents the eastward movement. Furthermore, the 3-dimension simulation models for wildebeest migration routes on sphere are shown in Figure 4.20.

### 4.3 Arctic tern migration

Arctic tern is a seabird which has the longest migration route in the world. Their migration routes not only have long distance between Greenland and Antarctica, but also have many patterns. Main informations of arctic tern migration are based on [4]. Moreover, we receive the tracking of arctic tern during their migration from [4]. The routes of arctic tern migration routes data from [4] are shown

in Figures 4.21 and 4.22.

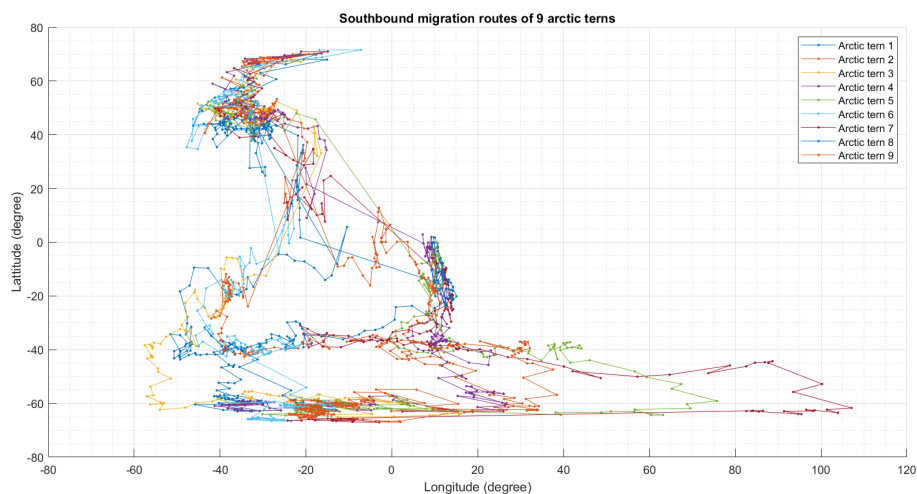


**Figure 4.21:** Southbound migration routes of arctic terns.

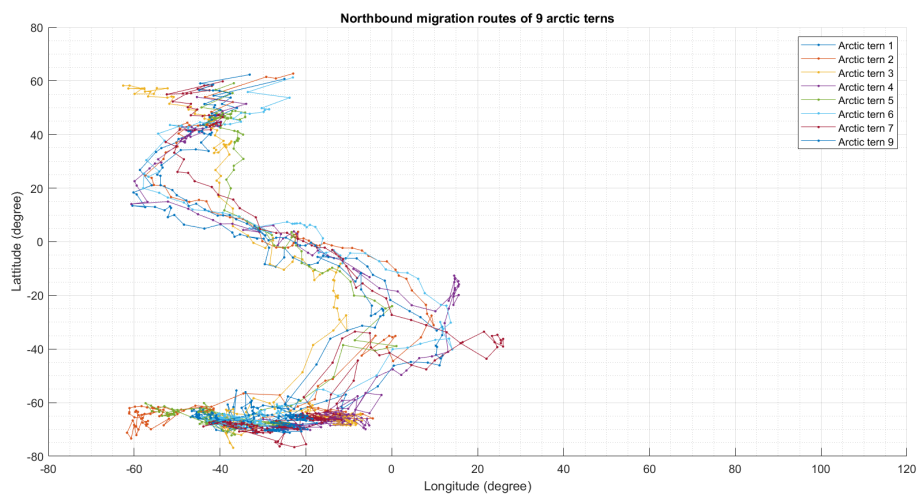


**Figure 4.22:** Northbound migration routes of arctic terns.

To describe their migration, all representative points are denoted as follows: GL = Greenland; SO(1), SO(2), SO(3) = Stopover; WS(1), WS(2) = Wintering site; and T1, T2, T3, T4(1), T4(2), T5(1), T5(2), T6, T7, T8 = Transit 1, 2, 3, 4(1), 4(2), 5(1), 5(2), 6, 7, 8, respectively. Their coordinates are shown in Table 4.3.

Representative points	Coordinates (degree)
GL	$(74.26^\circ, -20.16^\circ)$
SO	$(47^\circ, -34^\circ)$
WS	$(-58^\circ, -30.5^\circ)$
T1	$(10^\circ, -23.61^\circ)$
T2	$(-5^\circ, -31^\circ)$
T3	$(-5^\circ, 4^\circ)$
T4	$(-39^\circ, -47^\circ)$
T5	$(-39^\circ, 15^\circ)$
T6	$(-50^\circ, 106^\circ)$
T7	$(-22^\circ, 8^\circ)$
T8	$(16^\circ, -57^\circ)$

**Table 4.3:** The coordinates of representative locations.

We set the initial date and time of migration to be 10<sup>th</sup> August 2007 at noon and the end date and time to be 31<sup>st</sup> May 2008 at noon which gives  $T = 424800$ .

		Patterns									
n	$t_n$	1	2	3	4	5	6	7	8	9	10
0	0	GL									
1	17280	SO(1)									
2	51840	SO(2)									
3	74880	T1									
4	108000	T2					T3				
5	119520	T4(1)					T5(1)				
6	152640	WS(1)	T5(2)			WS(1)	T4(2)		T6		
7	161280		WS(1)				WS(1)		WS(1)		
8	360000	WS(2)									
9	368640	T7									
10	396000	T8									
11	400320	SO(3)									
12	407520	GL	SO(4)	GL	SO(4)	GL	SO(4)	GL	SO(4)	GL	SO(4)
13	424800		GL		GL		GL		GL		GL
Probability		1/8					1/12				

**Table 4.4:** The 10 patterns of arctic tern migration and their probabilities.

In the first half of their migration, they departed from GL and went to the SO(1) at time  $t_1$ ; all the discretized times are shown in Table 4.4. They stop at the SO(1) for a while, and then, at the time  $t_2$ , they continued downward to the south of the Cape Verde Islands (T1). At this area, they split into 2 groups at the time  $t_3$ . The first group crossed the Atlantic to East coast of Brazil (T2) while the second group flew along the West coast of African (T3) at the time  $t_4$ . After that, their movement was East-West through various locations, see Figure 4.23. At the time  $t_7$ , all birds went to WS(1) and stayed there for winter. The

northbound migration began at the time  $t_8$  from WS(2) to GL with a particular S-curve movement. At the time  $t_{11}$  at SO(3) some of them stayed there before went to GL while the others went straight to GL. Finally, all birds come back at GN at the time  $t_{13}$ .

We assume in this work that there are 10 possible patterns of arctic tern migration. We claim that at the time  $t_4$ , the arctic terns will go to T2 and T3 with equal probability of  $\frac{1}{2}$ ; at the time  $t_5$ , the birds at T4 will go WS and T5 with equal probability of  $\frac{1}{2}$ ; and the birds at T5 will go WS, T4 and T6 with equal probability of  $\frac{1}{3}$ . As for the northbound routes, at the time  $t_{11}$ , the birds continue upward to GL and stay at SO before go up to GL with equal probability of  $\frac{1}{2}$ . The discretized times and the pathways along with their probabilities of 10 different patterns are shown in Table 4.4.

For each pattern  $p$ , let  $0 = t_0 < t_1 < t_2 < \dots < t_{N_p-1} < t_{N_p} = T$ . The period  $[t_{n-1}, t_n]$  represents time interval of different behavior for  $n = 1, 2, \dots, N_p$ . For example, pattern 1 can occur with probability  $1/8$  that the birds go from GN to SO(1) at the time  $t_1$  and stay there for a while, i.e. shown as direction from SO(1) to SO(2). At the time  $t_2$  they move to T1, T2, and T4(1) at the time  $t_3, t_4$  and  $t_5$ , respectively. After that they travel toward to WS(1) for the winter at the time  $t_7$  and stay there until the time  $t_8$ , i.e. shown as direction from WS(1) to WS(2). Next, they fly through T7, T8, and SO(3) at the time  $t_9, t_{10}$  and  $t_{11}$ , respectively, and they continue to Greenland directly. The other patterns can also be described similarly.

The simulated migration routes of 100 arctic terns using  $\Delta t = 60$  and with suitable adjusted parameters  $\gamma_n, \sigma_n$ , and  $\hat{\sigma}$  (provided in Appendix) for each period, are below in Figures 4.24-4.31.



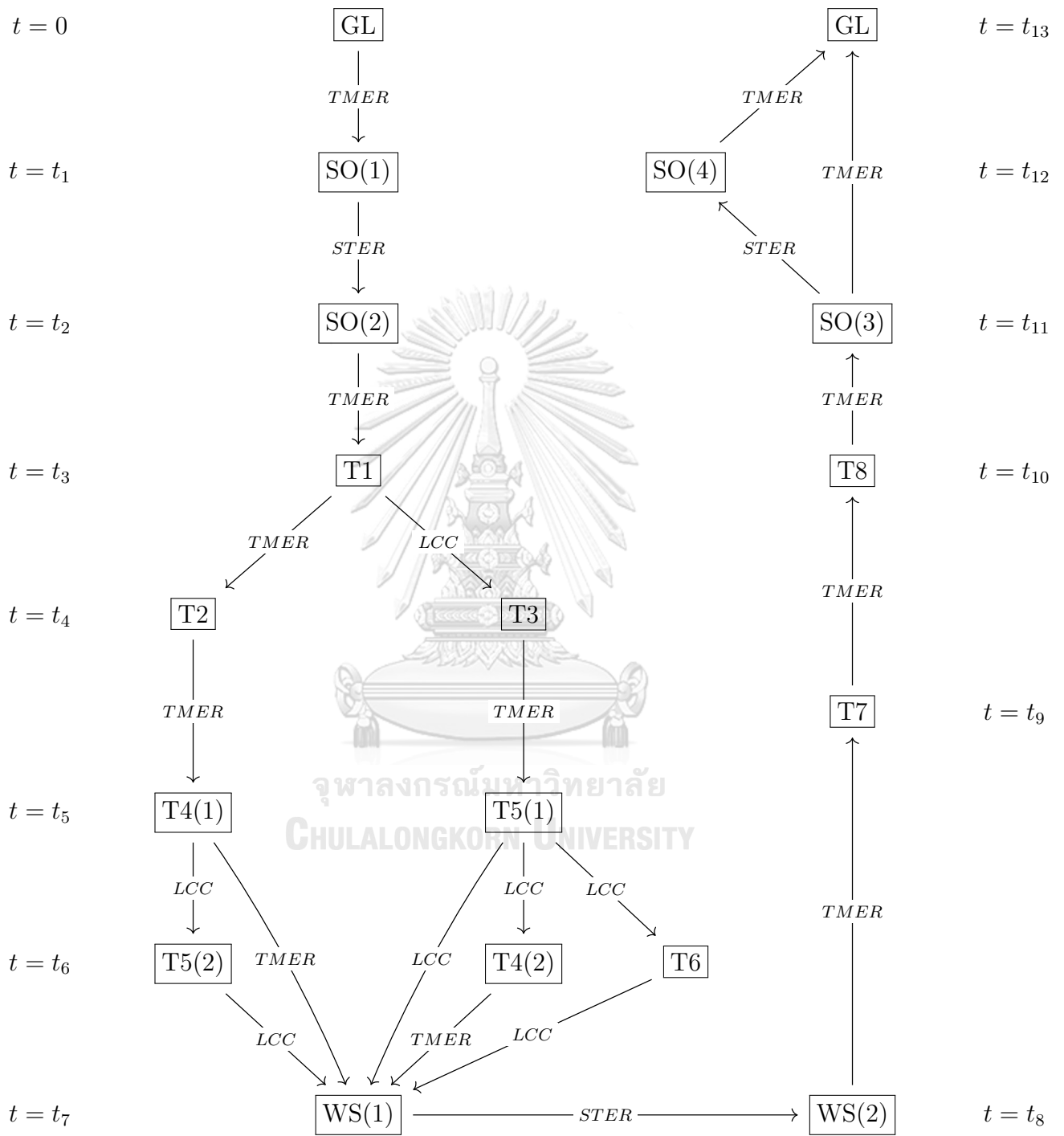


**Figure 4.23:** The routes of arctic tern migration for each period.

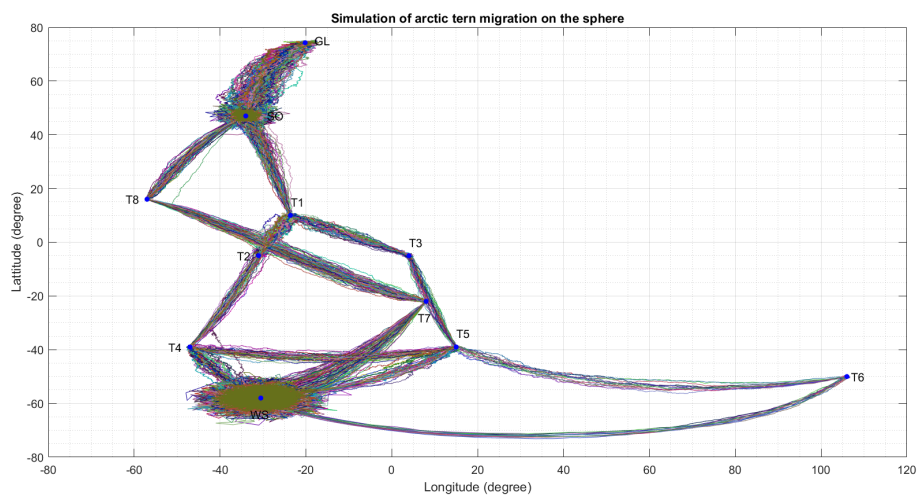


**Figure 4.24:** Coordinate  $(\phi, \theta)$  of simulation of the routes of arctic tern migration on the sphere.

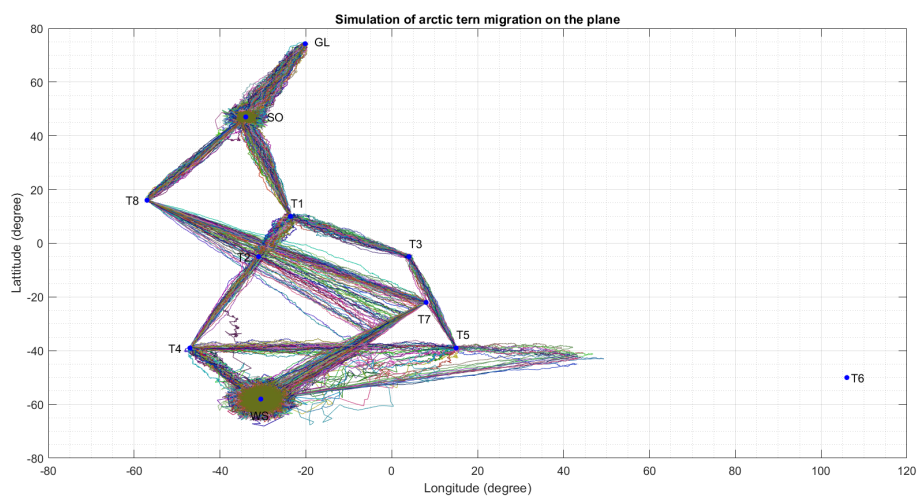


**Figure 4.25:** Coordinate  $(\phi, \theta)$  of simulation of the routes of arctic tern migration on the plane.

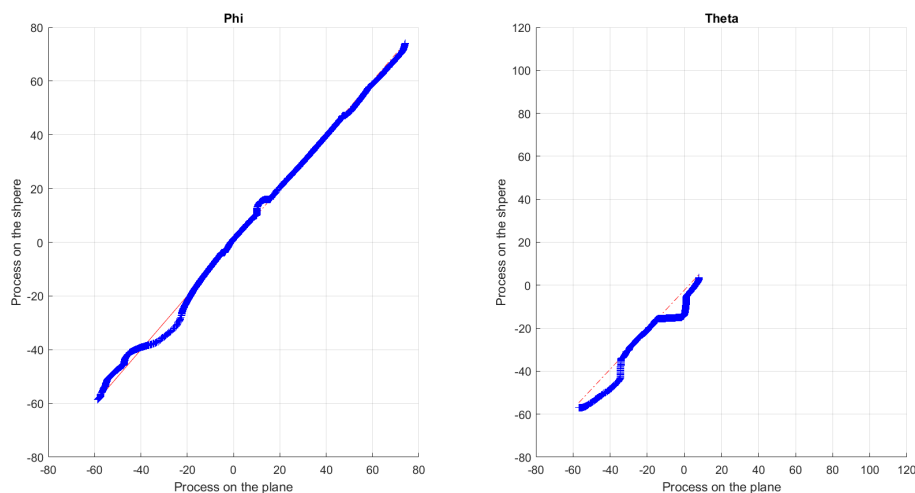
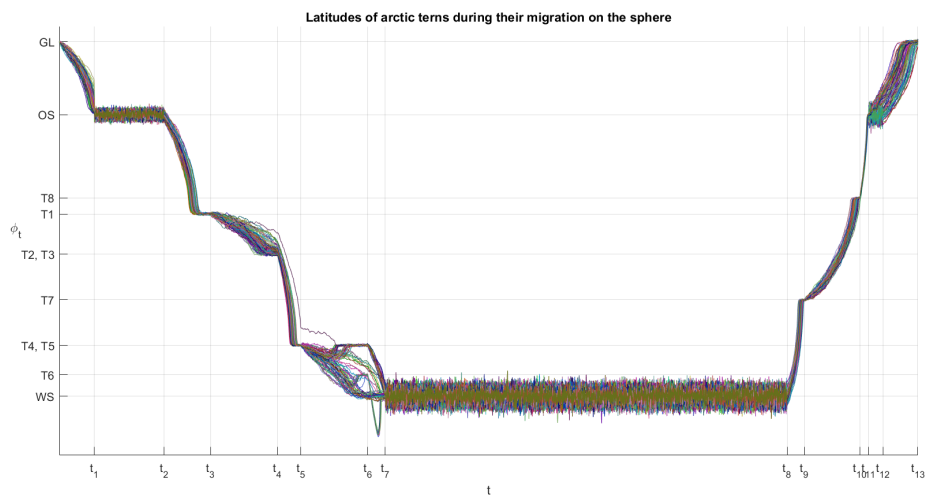


**Figure 4.26:** The Q–Q plots of processes on the plane and the sphere.

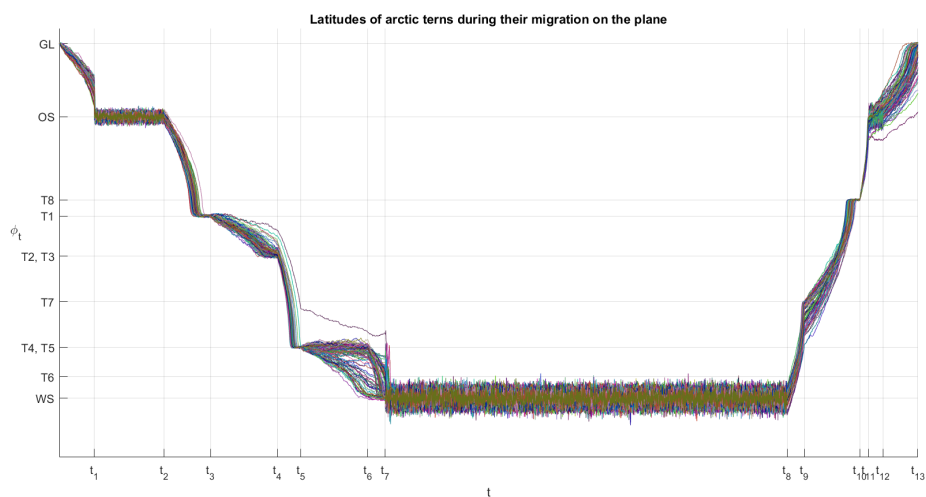
Figures 4.24 and 4.25 show all routes of patterns of arctic tern migration models on the sphere and the plane, respectively. The birds begin their southbound migration from Greenland, and split into 2 groups having different East-West movements. However, in the end of southbound migration, all birds go to wintering site near Antarctica. After that, they move northward with S-curve from wintering site to the stopover. At the stopover, some birds continue to Greenland directly, while the others pause there before continuing to Greenland.

Figure 4.26 shows distributions (Q–Q plots) between the mean path of the process on the plane compared with the mean path of the process on the sphere. This result shows that the paths of arctic terns for the longitude coordinate from the process on the plane is incomplete (right hand side of Figure 4.26) and different from that for the process on the sphere. This result agree with sample-paths shows in Figures 4.24-4.25, showing the difference between the paths between the sphere and plane processes. Moreover, as compared with real data (Figure 4.21), the simulation of arctic tern migration on the sphere provides more accurate result than that from the plane.

In addition, when compared arctic tern migration route with other short-distant animal migration routs such as sardine and wildebeest, we see that the modeling of long distant animal migration is required to perform on the sphere.



**Figure 4.27:** Latitude movement of 100 arctic terns modeled on the sphere.



**Figure 4.28:** Latitude movement of 100 arctic terns modeled on the plane.

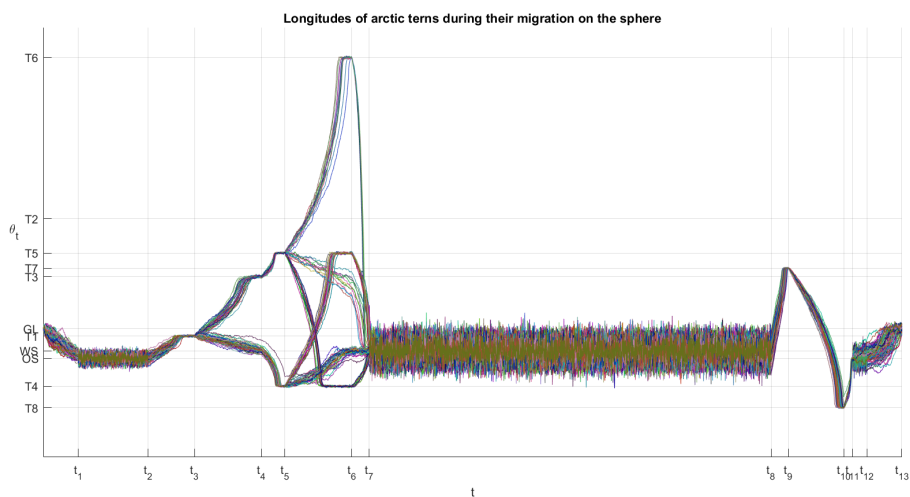


**Figure 4.29:** Longitude movement of 100 arctic terns modeled on the sphere.

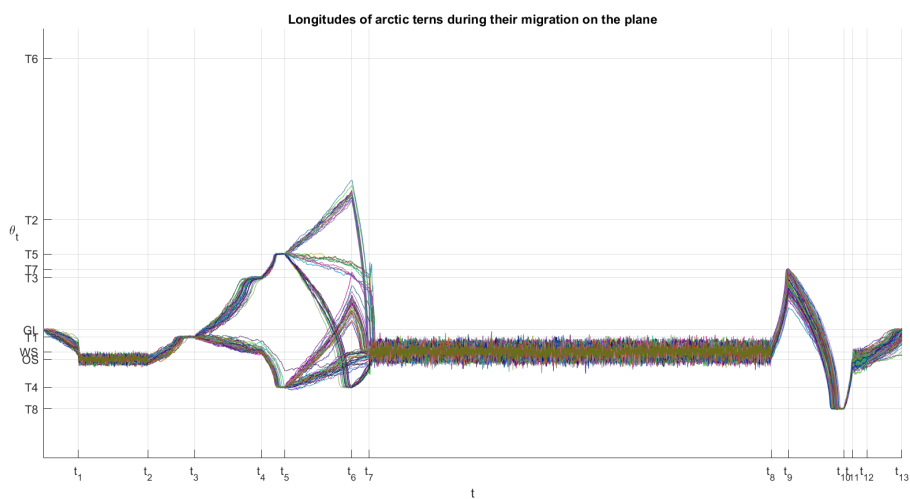


**Figure 4.30:** Longitude movement of 100 arctic terns modeled on the plane.

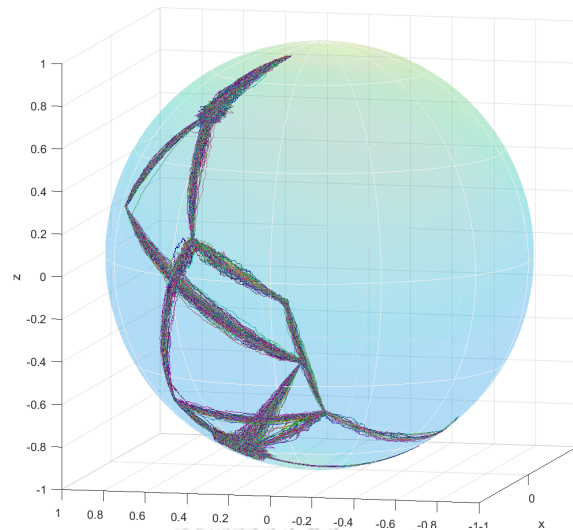


**Figure 4.31:** Simulation of arctic tern migration routes displayed on the sphere.

The latitude and longitude of simulation paths are shown in Figures 4.27-4.30. The North-South movement is considered according to the trend of latitude; the increasing of latitude represents the northbound movement, while the decreasing of latitude represents the southbound movement. Similarly, East-West movement is considered according to the trend of longitude; the increasing of longitude represents the eastbound movement while the decreasing of longitude represents the westbound movement. Furthermore, the 3-dimension simulation models for arctic tern migration routes on sphere are shown in Figure 4.31.

## CHAPTER V

### CONCLUSION AND FUTURE WORK

All simulations of animal migration routes are generated according to the proposed animal migration SDE models: the simulated routes of sardine run show the westward and northward movements along the South Coast and the East Coast of South Africa, respectively; the simulated wildebeest migration routes show the separated movements to difference areas—going to the transits sequentially and returning to the Ngorongoro Conservation Area; the simulated arctic tern migration routes follow the observed real data showing the separations of birds that go along the coast to the West African and move across to the East Coast of Brazil.

The appropriate map projections are applied for each movement period to establish the models. The STER, TMER, and LCC projections are suitable applied for surrounding movements, North-South movements, and East-West movements, respectively. In general, one can select any appropriate map projections to use in the models according to animal behaviors, distances and directions of movements.

The Q-Q plots of sardine run and wildebeest migration routes suggest that, for animal migration routes having not so large distances, the simulated migration routes generated on the sphere and the plane provide similar results. However, for long distant migration routes such as arctic tern migrations, the simulations should be modeled on the sphere, since there might be some distortions along the longitude coordinate for the simulations modeled on the plane; as for arctic turn in this study.

Indeed, reserved animals such as dugong (*Dugong dugon*), brow-antlered deer (*Rucervus eldii thamin*), and white-eyed river martin (*Pseudochelidon sirintarae*)

are unable to be tracked because of mistreatment. For this reason, if we have enough data and know the exact places and dates that they reach, our model is able to predict their location at any time after then.

For effectiveness for further modeling and simulation of animal migrations, additional related results and real observed data are required. This work contains partly facts of animal migrations, which can be used as a basic idea for developing more realistic animal migration models. We provided here 4 possible comments for future work as follows.

- 1) Boundary conditions can be included into the model. If we know animal movements in some specific area, we can create the boundary for that area and set the boundary condition for the SDE model. For example, arctic terns travel over the seas but not mainlands such as Africa, South America, and Antarctica; thus, we may set an appropriate boundary condition on the coastline of the mainlands.
- 2) The times of changing migration behaviors or routes,  $t_i$  in our model, can be randomly selected. In our model, these times are fixed for each animal according to the observed real data, so, all simulated routes change the movements abruptly at these times. We can fix these simultaneous movements by assigning suitable distributions for the periods of the migration behaviors, so that each individual simulated route has different times to change the migration behaviors.
- 3) The model can be generalized to have more than one attracting point in each behavior period. Moreover, we can have sources of dangers, such as natural enemies and storms, that can push away animals. For example, if we have



$m$  sources of incentives/dangers, the generalized model will have the form

$$d\phi_t = \sum_{i=1}^m \alpha_i(t) \left[ A_i(\phi_t, \theta_t)dt + B_i(\phi_t, \theta_t)dU_t + C_i(\phi_t, \theta_t)dV_t + G_i(\phi_t, \theta_t)d\hat{U}_t \right],$$

$$d\theta_t = \sum_{i=1}^m \alpha_i(t) \left[ D_i(\phi_t, \theta_t)dt + E_i(\phi_t, \theta_t)dU_t + F_i(\phi_t, \theta_t)dV_t + H_i(\phi_t, \theta_t)d\hat{U}_t \right],$$

comparing with Equations (3.7) and (3.8), where  $0 \leq \alpha_i(t) \leq 1$  and  $\sum_{i=1}^m \alpha_i(t) = 1$  for all time  $t$ ;  $\alpha_i(t)$  is a deterministic function that gives a weight of importance for the  $i^{th}$  incentive or danger at time  $t$ , thus, these functions  $\alpha_i$ 's can control the dynamic of the movement behaviors.

- 4) The parameter estimation can be implemented to obtain suitable parameters for the model. Unfortunately, available data for most animals are quite rare and inadequate to make a good estimation.

## REFERENCES

- [1] Hill JM, Sandercock BK, Renfrew RB (2019) Migration patterns of upland sandpipers in the western hemisphere. *Front Ecol Evol* **7**: 426.
- [2] van Toor ML, Hedenström A, Waldenström J, Fiedler W, Holland RA, Thorup K, et al. (2013) Flexibility of continental navigation and migration in European mallards. *PLoS One* **8**(8): e72629.
- [3] Exo KM, Hillig F, Bairlein F (2019) Migration routes and strategies of Grey Plovers (*Pluvialis squatarola*) on the East Atlantic Flyway as revealed by satellite tracking. *Avian Res* **10**: 28.
- [4] Carsten E, Iain JS, Richard AP, Aevan P, James WF, Janet RDS (2010) Tracking of Arctic terns *Sterna paradisaea* reveals longest animal migration. *Proceedings of the National Academy of Sciences Conference Proceedings*, 2010: pp. 2078–2081.
- [5] Yosida K (1949) Brownian motion on the surface of the 3-sphere. *Ann Math Statist* **20**: 292–296.
- [6] Le Gall JF, Yor M (1986) Étude asymptotique de certains mouvements browniens complexes avec drift. *Prob Th Rei Fields* **71**: 183–229.
- [7] Brillinger DR, Brent SS (1998) Elephant-seal movements: modelling migration. *Can J Stat* **26**: 431–443.
- [8] Rogers LCG, Williams D (2000) *Diffusions, Markov Processes, and Martingales*, Cambridge University Press, Cambridge.
- [9] Peter E, Kloeden EP (1992) *Numerical Solution of Stochastic Differential Equations*, Springer-Verlag, vol. 1, Berlin.

- [10] John PS (1987) *Map Projections: A Working Manual*, vol. 1, Washington, D.C.
- [11] Kennedy M, Steve K (2000) *Understanding Map Projections: GIS by ESRI*, vol. 1, Redlands.
- [12] Polyanin AD (2001) *Handbook of Linear Partial Differential Equations for Engineers and Scientists*, 1st edn, Chapman and Hall/CRC.
- [13] Coetzee JC, van der Lingen CD, Hutchings L, Fairweather TP (2008) Has the fishery contributed to a major shift in the distribution of South African sardine?, *ICES Marine Sci*, **65**: 1676–1688.
- [14] van der Lingen CD, Coetzee JC, Hutchings L (2010) Overview of the KwaZulu-Natal sardine run, *African Marine Sci*, **32**: 271-277.
- [15] *Spectacular Diving Experiences: The Sardine Run*. Available at :  
<https://www.animalsaroundtheglobe.com/sardine-run/>
- [16] *Great Wildebeest Migration Map*. Available at :  
<https://whileinafrica.com/the-great-wildebeest-migration-map/>
- [17] *Wildebeest Migration: The Complete Guide*. Available at :  
<https://www.animalsaroundtheglobe.com/wildebeest-migration-the-complete-guide/>



APPENDIX

จุฬาลงกรณ์มหาวิทยาลัย  
**CHULALONGKORN UNIVERSITY**

## 1. Parameters for SDE model and simulations

In the modeling and simulation described in chapter 4, we use  $\hat{\sigma} = 10^{-5}, 10^{-25}$ , and  $10^{-25}$  for sardine run, wildebeest, and arctic tern migrations, respectively, and  $\gamma_n$  and  $\sigma_n$  for all simulations are shown below.

		$\gamma_n$	$\sigma_n$
n	1	0.0000008	0.00001
	2	0.0000005	0.00003
	3	0.000001	0.00006

**Table 1:** Parameters  $\gamma_n$  and  $\sigma_n$  for sardine run migration model.

		Pattern			
		1	2	3	4
n	1	0.0000014	0.0000014	0.0000014	0.0000014
	2	0.0000025	0.0000025	0.0000025	0.0000025
	3	0.0000004	0.0000004	0.0000004	0.0000004
	4	0.0000025	0.0000025	0.0000025	0.0000025
	5	0.0000012	0.0000012	0.0000012	0.0000012
	6	0.0000006	0.0000006	0.0000006	0.0000006
	7	0.0000018	0.0000018	0.0000018	0.0000018
	8	0.0000005	0.0000005	0.0000005	0.0000005
	9	0.0000007	0.0000007	0.0000007	0.0000007
	10	0.0000015	0.0000015	0.0000015	0.0000015

**Table 2:** Parameter  $\gamma_n$  for wildebeest migration model.

		Pattern			
		1	2	3	4
n	1	0.000005	0.000005	0.000005	0.000005
	2	0.000003	0.000003	0.000003	0.000003
	3	0.000007	0.000007	0.000007	0.000007
	4	0.000009	0.000009	0.000009	0.000009
	5	0.00001	0.00001	0.00001	0.00001
	6	0.000008	0.000008	0.000008	0.000008
	7	0.000006	0.000006	0.000006	0.000006
	8	0.000004	0.000004	0.000004	0.000004
	9	0.000003	0.000003	0.000003	0.000003
	10	0.000008	0.000008	0.000008	0.000008

**Table 3:** Parameter  $\sigma_n$  for wildebeest migration model.

		Pattern									
		1	2	3	4	5	6	7	8	9	10
1	n	0.000007	0.000007	0.000007	0.000007	0.000007	0.000007	0.000007	0.000007	0.000007	0.000007
2		0.0001	0.0001	0.0001	0.0001	0.0001	0.0001	0.0001	0.0001	0.0001	0.0001
3		0.000015	0.000015	0.000015	0.000015	0.000015	0.000015	0.000015	0.000015	0.000015	0.000015
4		0.0000015	0.0000015	0.0000015	0.0000015	0.000006	0.000006	0.000006	0.000006	0.000006	0.000006
5		0.00003	0.00003	0.00003	0.00003	0.00003	0.00003	0.00003	0.00003	0.00003	0.00003
6		0.000003	0.000003	0.000015	0.000015	0.000002	0.000002	0.0000035	0.0000035	0.000002	0.000002
7		0.000001	0.000001	0.00002	0.00002	0.000009	0.000009	0.00001	0.00001	0.00001	0.00001
8		0.0001	0.0001	0.0001	0.0001	0.0001	0.0001	0.0001	0.0001	0.0001	0.0001
9		0.00005	0.00005	0.00005	0.00005	0.00005	0.00005	0.00005	0.00005	0.00005	0.00005
10		0.000037	0.000037	0.000037	0.000037	0.000037	0.000037	0.000037	0.000037	0.000037	0.000037
11		0.000055	0.000055	0.000055	0.000055	0.000055	0.000055	0.000055	0.000055	0.000055	0.000055
12		0.000008	0.0001	0.000008	0.0001	0.000008	0.0001	0.000008	0.0001	0.000008	0.0001
13		0.0000065	0.000009	0.0000065	0.000009	0.0000065	0.000009	0.0000065	0.000009	0.0000065	0.000009

**Table 4:** Parameter  $\gamma_n$  for arctic tern migration model.

		Pattern									
		1	2	3	4	5	6	7	8	9	10
1	n	0.0002	0.0002	0.0002	0.0002	0.0002	0.0002	0.0002	0.0002	0.0002	0.0002
2		0.002	0.002	0.002	0.002	0.002	0.002	0.002	0.002	0.002	0.002
3		0.0002	0.0002	0.0002	0.0002	0.0002	0.0002	0.0002	0.0002	0.0002	0.0002
4		0.0002	0.0002	0.0002	0.0002	0.0002	0.0002	0.0002	0.0002	0.0002	0.0002
5		0.0002	0.0002	0.0002	0.0002	0.0002	0.0002	0.0002	0.0002	0.0002	0.0002
6		0.0002	0.0002	0.0002	0.0002	0.0002	0.0002	0.0002	0.0002	0.0002	0.0002
7		0.0002	0.0002	0.0002	0.0002	0.0002	0.0002	0.0002	0.0002	0.0002	0.0002
8		0.004	0.004	0.004	0.004	0.004	0.004	0.004	0.004	0.004	0.004
9		0.0002	0.0002	0.0002	0.0002	0.0002	0.0002	0.0002	0.0002	0.0002	0.0002
10		0.0002	0.0002	0.0002	0.0002	0.0002	0.0002	0.0002	0.0002	0.0002	0.0002
11		0.0003	0.0003	0.0003	0.0003	0.0003	0.0003	0.0003	0.0003	0.0003	0.0003
12		0.0004	0.0035	0.0004	0.0035	0.0004	0.0035	0.0004	0.0035	0.0004	0.0035
13		0.0002	0.0002	0.0002	0.0002	0.0002	0.0002	0.0002	0.0002	0.0002	0.0002

**Table 5:** Parameter  $\sigma_n$  for arctic tern migration model.



## BIOGRAPHY

**Name** Mr. Viput Puttanugool

**Date of Birth** 16 September 1995

**Place of Birth** Saraburi, Thailand

**Education** B.S. (Mathematics),  
Chulalongkorn University, 2018

